SANDIA REPORT

SAND97–0619 • UC–606
Unlimited Release
Printed March 1997

Metal-Loaded Polymer Films for Chemical Sensing of ES&H-Related Pollutants

Stephen J. Martin, Gregory C. Frye

Prepared by
Sandia National Laboratories
Albuquerque, New Mexico 87185 and Livermore, California 94550

Sandia is a multiprogram laboratory operated by Sandia Corporation, a Lockheed Martin Company, for the United States Department of Energy under Contract DE-AC04-94AL85000.

Sandia National Laboratories

Issued by Sandia National Laboratories, operated for the United States Department of Energy by Sandia Corporation.

Available to DOE and DOE contractors from
Office of Scientific and Technical Information
P.O. Box 62
Oak Ridge, TN 37831

Prices available from (615) 576-8401, FTS 626-8401

Available to the public from
National Technical Information Service
U.S. Department of Commerce
5285 Port Royal Rd
Springfield, VA 22161

NTIS price codes
Printed copy: A04
Microfiche copy: A01

SAND97-0619
Unlimited Release
Printed March 1997

Distribution
Category UC-606

Metal-Loaded Polymer Films for Chemical Sensing of ES&H-Related Pollutants

Stephen J. Martin and Gregory C. Frye
Microsensor Research and Development Department
Sandia National Laboratories
P.O. Box 5800
Albuquerque, New Mexico 87185-1425

ABSTRACT

This report summarizes the results of a Laboratory Directed Research and Development (LDRD) effort to study and model surface acoustic wave (SAW) devices for environmental applications. The response of polymer-coated SAW devices to temperature changes and polymer vapor absorption is examined. A perturbational approach is used to relate velocity and attenuation responses to film translational and strain modes generated by the SAW. Two distinct regimes of film behavior arise, causing different SAW responses. For glassy films, displacement is nearly uniform across the film thickness, varying only in the direction of propagation. A model developed to predict velocity and attenuation in this regime (Model 1), reduces to the familiar Tiersten (Wohltjen) equation for purely elastic films. For elastomeric (rubbery) films, inertial effects cause a phase lag to occur across the film for shear displacements. A model to account for these cross-film displacement gradients (Model 2) predicts a characteristic resonant response when the film phase shift reaches np/2, where n is an odd integer. These model predictions are compared with measured responses from polyisobutylene-coated SAW devices as temperature is varied and during exposure to high vapor concentrations.

INTRODUCTION

In this project, we proposed the use of metal-loaded polymer films as chemically-sensitive layers on surface acoustic wave (SAW) devices. Small metal particles can be dispersed in polymer films. When the concentration of these particles is such that adjacent particles touch, the electrical conductivity of the films is high. When the film is exposed to a vapor that is absorbed the polymer, swelling of the polymer occurs, resulting in a greater separation between particles and a significant reduction in film conductivity. This can be used as a basis for constructing chemical sensors.

In this project, we proposed using the SAW device as a "platform" for detecting changes in metal-loaded polymer films due to vapor absorption. These devices are extremely sensitive to changes in film conductivity. As the film passes through a critical conductivity, attenuation goes through a maximum, while wave velocity changes drastically. By incorporating these devices in an oscillator circuit, very minute changes in film conductivity can be measured.

In coating SAW devices with polymer films, we found that there were other effects, aside from film conductivity changes, that lead to a sensor response. As a vapor is absorbed into a polymer, the mass density of the polymer changes. In addition, very large changes in the film's viscoelastic properties arises due to film "plasticization" by the absorbed vapor. The majority of the activity in this project was spent in characterizing the response of the SAW device to changes in film viscoelastic properties. A model was derived for the response of the SAW device with a viscoelastic film overlay. The response of polymer-coated SAW devices was also measured as viscoelastic properties were changed due to (1) temperature changes, and (2) vapor absorption. This report describes our efforts to characterize the response of the polymer-coated SAW device.

BACKGROUND

Surface acoustic wave (SAW) devices use interdigital transducers photolithographically patterned on the surface of a piezoelectric crystal (Fig. 1) to excite and detect surface waves[1]. These waves are excited in a frequency band centered at $f_o = v/d$, where v is the SAW propagation velocity and d is the transducer period. The SAW wavelength Λ generated at f_o matches the transducer period d. SAW devices typically operate in the 30 - 300 MHz range and use ST-cut[2] quartz substrates for high temperature stability near room temperature. In the delay-line device configuration[3], input and

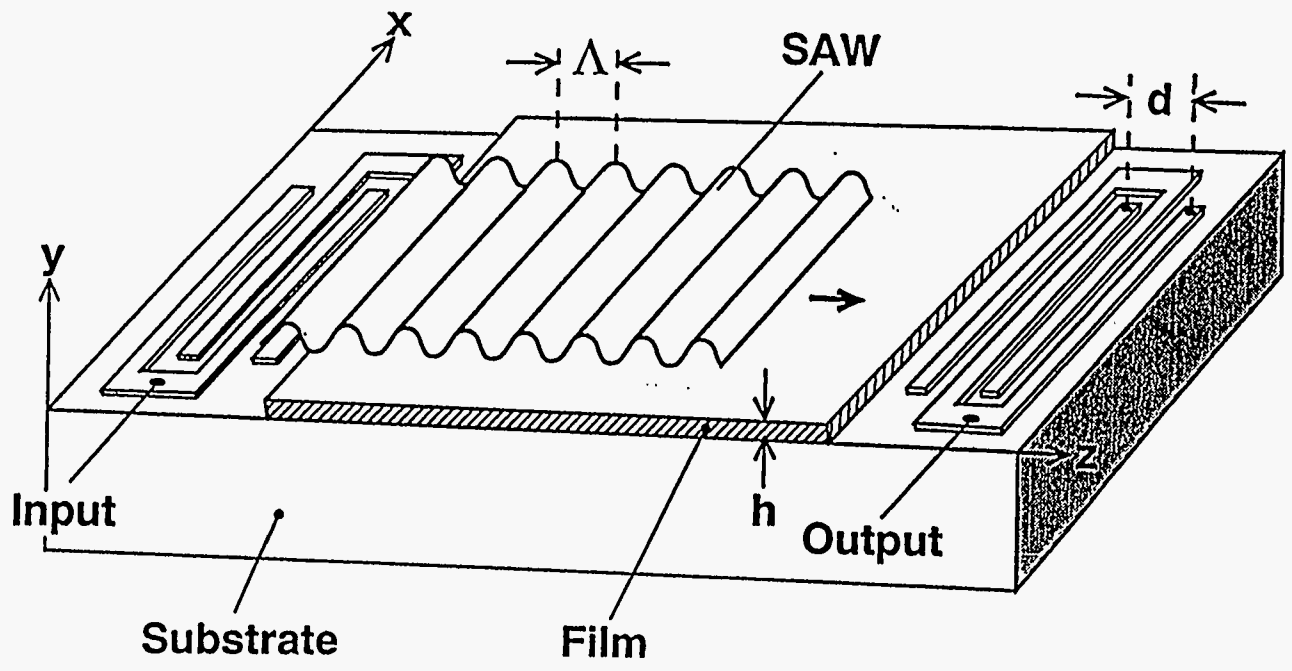

Fig. 1. Schematic of a surface acoustic wave (SAW) device with a polymer film coating.

T307A.BW3793.03

output transducers are typically separated by 100 - 200 wavelengths.

The extreme sensitivity of SAW devices to thin film properties has been used both (1) to characterize thin film elastic and viscoelastic properties[4], and (2) to construct gas and vapor sensors[5]. In these applications, a thin film (thickness $h \ll \Lambda$) is coated on the substrate in the region between transducers (Fig. 1). If the film is nonconductive, the film may coat the transducers also. Thin film elastic and viscoelastic properties are studied by using the SAW to deform the film, thereby *probing* its mechanical properties. A chemical sensor results when interaction between the film and a vapor or chemical species modifies the SAW behavior. In both applications, changes in film properties induce two changes in SAW propagation characteristics: velocity and attenuation (rate of amplitude decay).

Since the invention of SAW chemical sensors by Wohltjen[6], a number of polymer films have been examined as chemically sensitive films[7] or "chemical interfaces." This is due to the wide range of chemical properties available and the ease of film formation: polymer films can be deposited from solution by spin-casting, air-brushing, or dip-coating; certain ones can also be formed by plasma deposition[8]. As a chemical interface, the film, in effect, *dissolves* gas-phase species, maintaining a film concentration in equilibrium with the gas phase concentration. The dissolved species contributes added mass and may, in addition, modify the mechanical properties of the film.

The mechanical properties of a linear, isotropic polymer can be specified by a bulk modulus K and a shear modulus G. Under sinusoidal deformation, these are represented as complex quantities[9]: $K = K' + jK''$ and $G = G' + jG''$. The real parts of K and G represent the component of stress in-phase with strain, giving rise to energy storage in the film (consequently K' and G' are referred to as *storage moduli*); the imaginary parts represent the component of stress 90° out of phase with strain, giving rise to power dissipation in the film (thus, K'' and G'' are called *loss moduli*). An ideal *elastic* film would have $K'' = G'' = 0$.

Polymers exhibit a wide range of viscoelastic properties that depend on the temperature and frequency of measurement. If deformed on a time scale short compared with the time for segmental chain motion τ, strain is accommodated elastically through chain deformations; this is the *glassy* regime, characterized by $G' \cong 10^{10}$ dyne/cm^2 and $G'' \ll G'$. If deformed on a time scale longer than

τ, strain is accommodated inelastically by interchain motion; this is the *rubbery* regime, characterized by $G' \leq 10^8$ dyne/cm^2 and G'' comparable to or less than G'. Thus, when probing at a given (angular) frequency ω, the material behaves as glassy if $\omega\tau \gg 1$ and rubbery if $\omega\tau \ll 1$. When $\omega\tau \approx 1$, there is a peak in K'' and G''. Since τ is strongly dependent on temperature, varying temperature can cause this transition from elastic to viscoelastic behavior. The temperature of this transition is the *dynamic glass transition temperature* T_g. Since this glass transition temperature is defined by $\tau(T_g) = 1/\omega$, the dependence of T_g on measurement frequency is apparent[10].

There are two quasi-static phenomena associated with the glass transition that are not observable at the high frequencies at which SAW devices operate. These are (1) an increase in specific heat as observed in DSC, and (2) an increase in thermal expansion coefficient. The latter has an indirect influence on SAW performance through changes in film thickness. Therefore, it is important to identify the temperature at which these quasi-static effects occur. The expression "static glass transition," denoted herein as $T_g^{(0)}$, is conventionally used, although it must be noted that measurements of $T_g^{(0)}$ are done by scanning methods, and therefore should be thought of as T_g in the limit of low frequency. $T_g^{(0)}$ and T_g can differ significantly; for example, in the PIB films used here $T_g^{(0)} = -68$°C, while T_g at 100 MHz is 40°C.

Although glass transitions have reportedly been observed in the response of polymer-coated SAW devices[11] (including the present authors[12]), this interpretation has been correctly challenged by Grate et al.[13]. Changes in the intrinsic polymer properties known to occur at T_g, specifically a rapid decrease in shear storage modulus (G') and a peak in shear loss modulus (G''), have usually been assumed to appear directly as changes in SAW velocity and attenuation[12]. Under this assumption, peaks in attenuation or velocity slope changes with temperature have been used to indicate T_g. However, it will be shown in this paper that velocity and attenuation changes track intrinsic properties only in extremely thin films (defined below). In this limit, attenuation peaks and velocity slope changes do coincide with T_g. For thicker films, however, the acoustic coupling to the film varies strongly with film thickness due to film interference effects. In this case, velocity and attenuation do *not* track changes in the intrinsic properties directly and, therefore, care must be used in inferring glass transitions from SAW velocity and attenuation responses.

SAW velocity and attenuation responses arise from the mechanical interaction that occurs

between the SAW and the film overlay. A film that is rigidly bonded to the surface of the piezoelectric substrate undergoes both translation and deformation under the influence of the propagating wave. Translation creates, in effect, mass loading on the SAW device, which decreases the SAW propagation velocity. In addition, the deformation produces energy storage in the film, which results in a change in SAW propagation velocity, and power dissipation in the film, which causes wave attenuation.

The wave energy stored and dissipated in the film depends upon the strain modes generated by the SAW in the film. Two distinct regimes of film behavior can be identified. Films that are thin and rigid behave as *acoustically thin*: the entire film moves synchronously with the substrate surface, resulting in uniform displacement across the film thickness. Films that are thick or soft behave as *acoustically thick*: the upper film portions lag behind the film/substrate interface, causing non-uniform displacement across the film thickness. Since the strain modes generated in each regime are different and result in distinct device responses, it is essential to understand the regime of operation for any particular measurement.

Tiersten and Sinha[14] derived a perturbational formula relating SAW velocity to film properties for the case of an acoustically thin, *elastic* film (see Eq. 6 below). This model has been shown to accurately predict SAW velocity changes arising from metallic[15], crystalline[16], or very thin polymer films[17]. Since translation and deformation of a purely elastic film is non-dissipative, no film-induced attenuation is predicted by this model.

Wohltjen first applied the Tiersten formula to interpret the response of polymer-coated SAW sensors[18]. Thus, the equation is commonly referred to in SAW sensor literature as the "Wohltjen equation." The dominant contribution to the SAW velocity response was assumed to arise from the mass of gas or vapor molecules absorbed into the film--the so-called "gravimetric" or "mass loading" response. While providing a good starting point for understanding SAW sensors, recent studies have indicated inadequacies in this model (as applied to polymer films) and called into question the dominance of mass loading in determining the SAW vapor response. For example, significant attenuation responses have been observed during vapor absorption[12,19]. Also, SAW velocity can decrease in some regimes of gas phase concentration while increasing in others. From thermodynamic arguments, the concentration of absorbed species is expected to increase

monotonically with gas-phase concentration. Thus, the non-monotonic velocity response (i.e., sign change) contradicts the mass-loading interpretation.

Several researchers have shown that a non-gravimetric response arises from polymer *plasticization*[20] or vapor-induced softening. Grate *et al.* [21], comparing SAW responses with chromatographic studies of polymer film absorption, found that the SAW velocity response was four times too large to be accounted for by the mass of absorbed species alone. They proposed "swelling-induced modulus changes" as the origin of the additional velocity change[22].

The difficulties in reconciling predicted and measured responses arises from the fact that the assumptions underlying the Tiersten model are rarely satisfied by polymer films. First, the *viscoelastic* nature of polymer films causes elastic energy to be both stored and dissipated during film deformation. This results in a significant contribution to SAW attenuation that is neglected in the Tiersten model. Second, the large change in viscoelastic properties undergone by polymers, either due to temperature change or vapor absorption, can cause even films satisfying $h \ll \Lambda$ (the criterion typically applied for invoking the Tiersten model) to behave as *acoustically thick*. This is because the film can be significantly softer than the substrate, resulting in a displacement variation across the film on a scale much smaller than Λ. This violates the assumption of synchronous film motion implicit in the Tiersten model.

In this paper, we investigate the dynamics and response of polymer-coated SAW devices, examining separately the acoustically thin and thick regimes. We begin with a criterion for separating these two regimes and examine the film strain modes that arise in each. A perturbational approach[23] is used to obtain explicit, although approximate, expressions for film-induced velocity and attenuation changes in each regime. In this approach, velocity and attenuation changes caused by the film are related to the surface mechanical impedances (a measure of the difficulty in displacing the film) contributed by the film. These mechanical impedances depend on the film properties and the detailed manner in which the film is translated and deformed by the passing wave. Changes in film viscoelastic properties induced by temperature changes and vapor absorption are expressed in terms of polymer free volume. Incorporating these film property changes into the models yields predictions for velocity and attenuation responses. These predictions are compared with experimental measurements made on polyisobutylene-coated SAW devices operating at 97

MHz. The best agreement is obtained using the acoustically thick model that accounts for cross-film displacement variations.

THEORY

A surface acoustic wave (SAW) in an uncoated substrate is formed by coupled compressional and shear waves propagating together to satisfy the stress-free boundary condition at the surface. Propagation of the SAW in the z-direction results in a displacement $\vec{u}$ of particles from their equilibrium position that varies with depth y into the crystal as

$$\vec{u}(x,y,z,t) = e^{(j\omega t-\gamma z)} \sum_{i=1}^{3} u_i(y)\, e^{j\psi_i} \hat{x}_i \qquad (1)$$

where $j = (-1)^{1/2}$; ω is the angular frequency ($2\pi f$); t is time; γ is a complex propagation factor; $u_x(y)$, $u_y(y)$, and $u_z(y)$ represent depth-dependent displacements in the x-, y-, and z-directions (values at the surface are denoted u_{xo}, u_{yo}, and u_{zo}); ψ_i are the relative phases of these components with respect to u_z; $\hat{x}_i$ are unit vectors in the x_i-direction. The amplitude components $u_i(y)$ decay exponentially with distance into the substrate so that most of the wave energy is confined to within one wavelength of the surface. The complex propagation factor in Eq. 1 is comprised of two components: $\gamma = \alpha + jk$. The attenuation, α, describes the rate of diminution in wave amplitude with distance; the wavenumber, k_o, describes the oscillatory portion of the wave motion: $k = \omega/v$, where v is the propagation velocity in the uncoated substrate.

Film Strains Induced by a Surface Acoustic Wave

When a thin film ($h \ll \Lambda$) is coated on the SAW substrate, the SAW surface displacements (u_{xo}, u_{yo}, u_{zo}) are, to first order, unchanged. SAW propagation thus causes a periodic displacement field to be imposed on the lower film surface: u_{xo} lies in the plane of the surface and normal to the direction of propagation, u_{yo} is normal to both the surface and the direction of propagation, while u_{zo} lies in the direction of propagation. This displacement field causes translation of the film and induces strains in the film.

Strain, defined as the symmetric gradient of displacement[24]

$$S_{ij} = \frac{1}{2}\left(\frac{\partial u_i}{\partial x_j} + \frac{\partial u_j}{\partial x_i}\right) \tag{2}$$

arises whenever there is a spatial variation or *gradient* ($\partial u_i/\partial x_j$) in a displacement component u_i. The surface displacement field has two distinct means of inducing strain in a film overlay: (1) from the in-plane gradients arising *due to the sinusoidal variation in displacement components along the direction of propagation* (the exp(-γz) term in Eq. 1), and (2) from surface-normal gradients arising *from inertial lag of the upper film portions* with respect to the "driven" lower film surface.

Fig. 2a shows the deformation arising in an acoustically thin film. Displacements u_i are constant across the film thickness, and only gradients *in the plane* of the film arise. The gradient in u_x leads to regions of compression and tension in the film, while the gradient in u_y lead to bending. Fig. 2b shows the deformation in an acoustically thick film. Displacement varies not only in the plane of the film but also across the film due to inertial lag of the upper film regions. The deformation in an acoustically thick film arises from a combination of both in-plane and cross-film gradients, with cross-film gradients dominating. As shown in Fig. 2b, the gradient in u_x across the film leads to shear deformation of the film. The regimes in which in-plane and cross-film gradients dominate and the corresponding velocity and attenuation changes will be considered below.

The mechanical interaction of the wave with the film results in a perturbation $\Delta\gamma$ of the complex wave propagation factor γ. In normalized form, this is[25]:

$$\frac{\Delta\gamma}{k_o} = \frac{\Delta\alpha}{k_o} - j\frac{\Delta v}{v_o} \quad . \tag{3}$$

Eq. 3 yields two measurable responses: the change in attenuation per wavenumber, $\Delta\alpha/k_o$, and the fractional change in propagation (phase) velocity, $\Delta v/v_o$. Eq. 3 also indicates that the attenuation change *divided by wavenumber* is the normalized complement to the commonly measured $\Delta v/v_o$ response.

Criterion for Separating Acoustically Thin and Thick Films

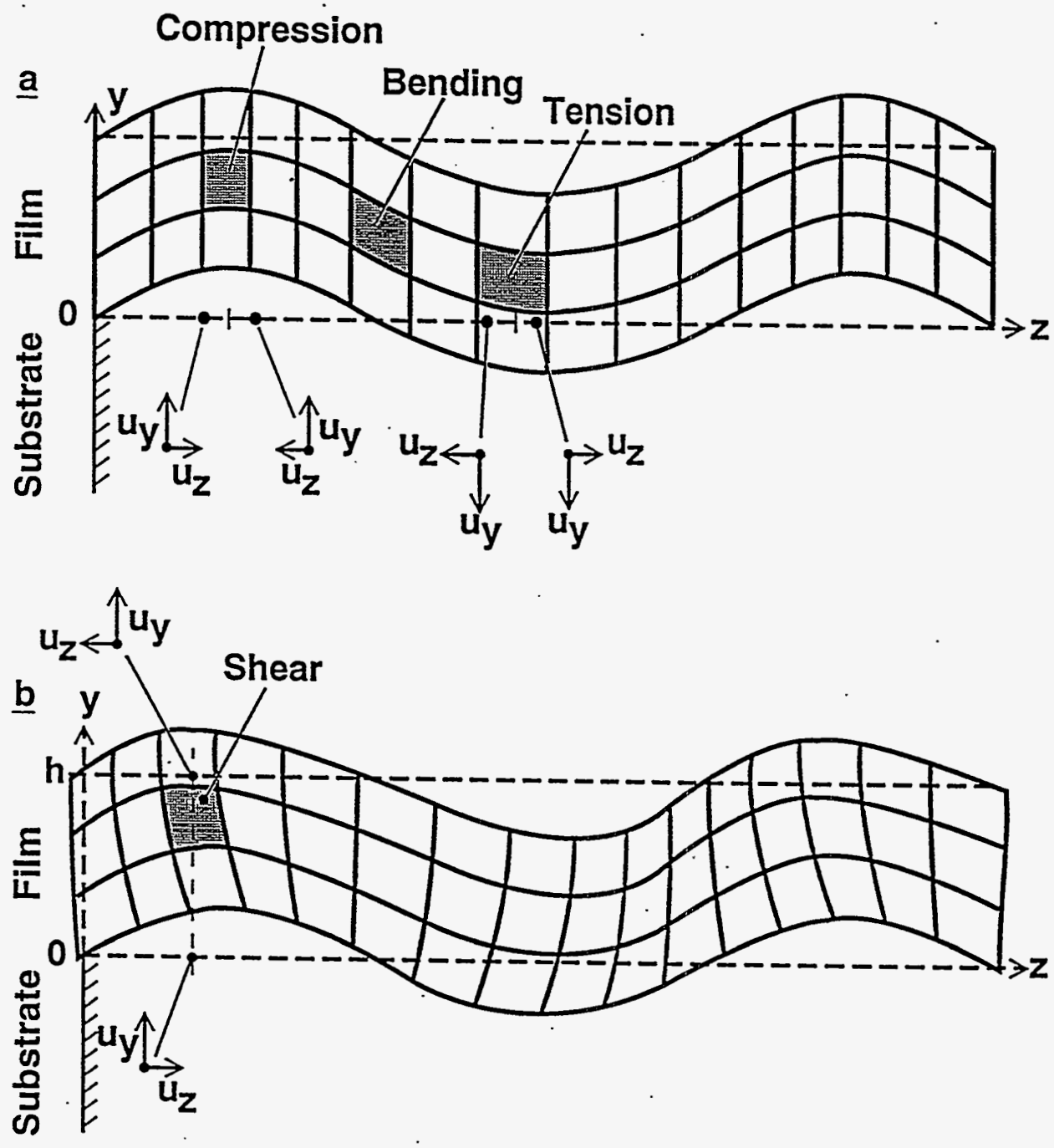

Fig. 2. Deformation generated by a SAW (a) in an acoustically thin ($R \ll 1$) film, in which in-plane displacement gradients [caused by sinusoidal variation in direction of propagation] dominate, and (b) in an acoustically thick ($R \geq 1$) film, where cross-film gradients [due to inertial lag in the film] also arise.

The ratio of film strains generated by cross-film displacement gradients to those generated by in-plane gradients is calculated (Appendix B) as

$$R = \frac{A f v_o \rho h}{|G|} \tag{4}$$

where ρ, h, and G are the film density, thickness, and shear modulus and A is a substrate-dependent parameter (see Appendix B) having a value of 1.9 for ST-cut quartz. When the film coating is sufficiently thin (small h) and rigid (large $|G|$) in comparison to the oscillation frequency, such that $R \ll 1$, in-plane gradients dominate over surface-normal gradients and the film is *acoustically thin* (Fig. 2a). When film properties are such that $R \geq 1$, inertial lag becomes significant so that surface-normal gradients are dominant (Fig. 2b), and the film is *acoustically thick.*

Fig. 3 shows the variation in R with the magnitude of the film shear modulus for various values of the quantity $fh\rho$ ($v_o \cong 3.2 \times 10^5$ cm/s); $|G|$ is displayed on a reversed logarithmic scale to mimic the way in which polymer properties vary with increasing temperature or vapor absorption. For devices operating at 100 MHz (typical SAW frequency) and coated with films having a density of 1 g/cm^3, the parentheses identify the corresponding film thickness. The curves in Fig. 3 indicate that as polymers undergo a glass-to-rubber transition, traversing the G' values along the abscissa from left to right, strains due to in-plane gradients are increasingly dominated by inertially-induced cross-film gradients. A 0.1 μm-thick polymer film on a 100 MHz device, for example, behaves as acoustically thin ($R \ll 1$) in the glassy state ($G' \approx 10^{10}$ dyne/cm^2), but behaves as acoustically thick ($R \geq 1$) in the rubbery state ($G' \leq 10^8$ dyne/cm^2). For thinner films, the modulus range over which the film behaves as acoustically thin is wider. However, only films with h < 20 nm (at 100 MHz) remain thin all the way into the rubbery regime. Polymer films with h ≥ 2 μm behave as acoustically thick even in the glassy state.

Strain Modes in Acoustically Thin Films

If the film is acoustically thin ($R \ll 1$), then u_x, u_y, u_z are constant across the film thickness, and only gradients *in the plane* of the film arise. The SAW-induced film deformation can be decomposed into three translations (in the x-, y-, and z-directions) and three strain modes. (Non-zero

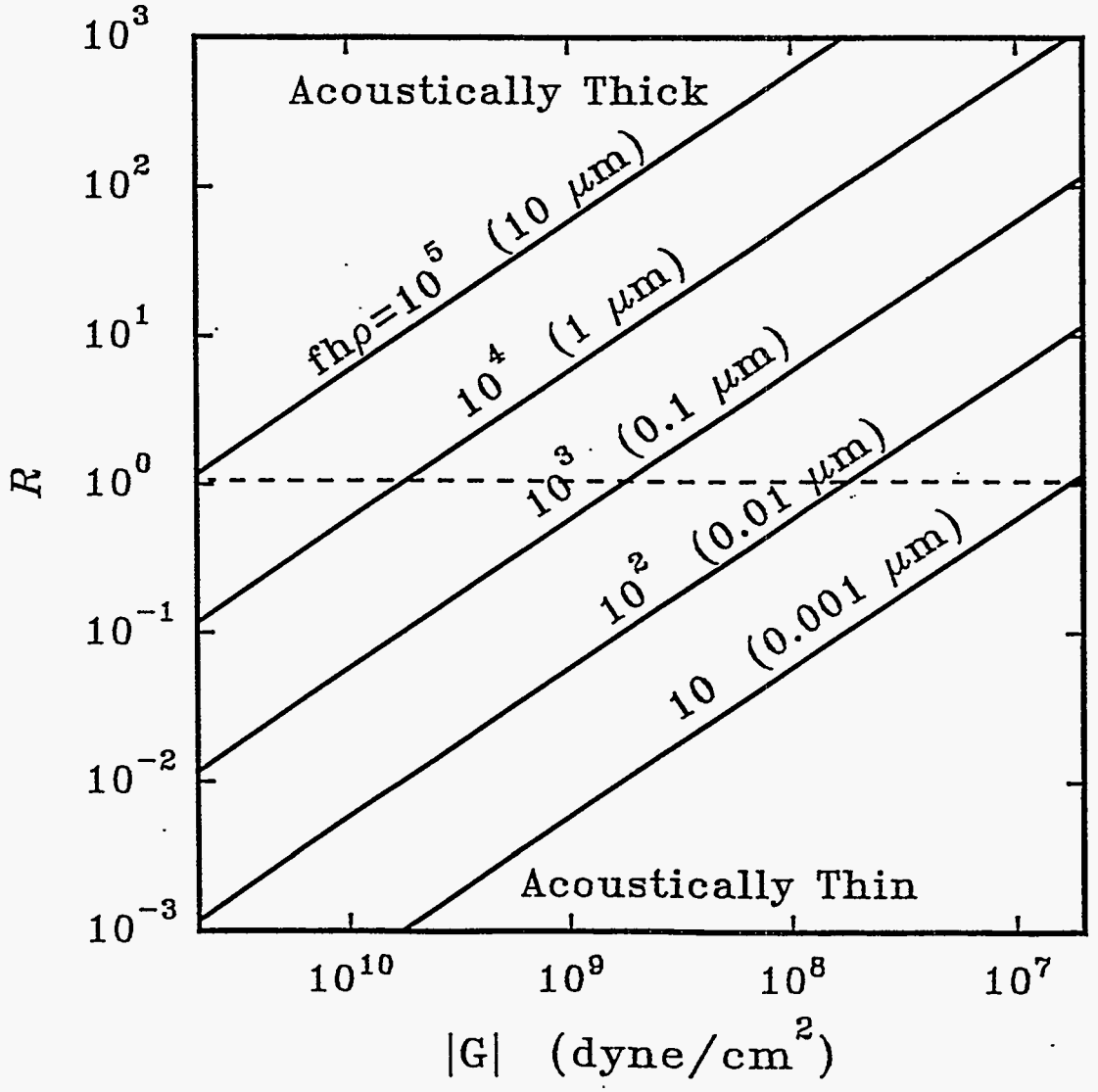

Fig. 3. Ratio R of in-plane to cross-film displacement gradients vs. $|G|$ at various values of $fh\rho$ (values in parentheses are film thickness for f = 100 MHz and ρ = 1 g/cm^3).

$\partial u_i/\partial z$ in Eq. 2 leads to S_{i3} strains.) These strains generate periodic compression, tension, and bending in the film, as shown in Fig. 2a, as well as transverse shear (not shown). The strain can be separated into distinct modes generated by each surface displacement component u_{io}, as shown in Fig. 4. Each strain mode arises from interfacial *stresses* imposed on the film by the wave. Since the film is acoustically thin, gradients in the direction of propagation impose stresses T_{i3} (force per area in the i^{th} direction in planes parallel to the direction of propagation--*z*) on the film. This produces reaction stresses that act on the wave and perturb its propagation velocity and attenuation. An important parameter in determining the contribution of each strain mode in perturbing SAW propagation is the modulus $E^{(i)}$--the ratio of stress to strain associated with each strain mode in Fig. 4. These moduli are listed in Table I in terms of the intrinsic elastic properties of the film, represented in terms of the Lame' constants (λ,μ) and the bulk and shear moduli (*K*,*G*). These sets of moduli are interrelated[26].

The strain modes generated in an acoustically thin film and the associated moduli $E^{(i)}$ are:

a. The gradient in u_x ($\partial u_x/\partial z$) generates a *transverse shear* (a change of angle in each volume element) in the plane of the film, as shown in Fig. 4a. The modulus for this shear deformation mode, listed in Table I, is $E^{(1)} = T_{13}/(2S_{13}) = G$. Thus, this mode probes only the in-plane shear modulus *G* of the film.

b. The gradient in u_y ($\partial u_y/\partial z$) causes a *bending moment*[27] to be imposed on the film (Fig. 4b). If we imagine the film detached from the substrate, it is apparent that it is easier to achieve displacement normal to the film (a bending motion) than in the plane of the film (a stretching motion). The modulus for this bending mode, $E^{(2)} = T_{23}/(2S_{23})$, is proportional to $(h/\Lambda)^3$, and is thus normally *negligible* in comparison with modes a and c. That is, the effect of this strain mode on SAW propagation is not generally observed.

c. The gradient in u_z ($\partial u_z/\partial z$) causes *longitudinal tension* (or compression) of the film along the direction of wave propagation (*z*), as shown in Fig. 4c. Since the film is unconstrained in the *y*-direction, this induces a transverse strain of opposite sign in this direction (the Poisson effect): the film expands (contracts) in the *y* direction due to compression (elongation) along the *z* direction. No strain occurs along the *x*-direction since the film is adhered to the substrate surface. Consequently,

Table I. Moduli associated with the strain modes (Fig. 4) generated by a SAW in an acoustically thin film ($R \ll 1$).

Strain Mode	Displacement Gradient	Modulus Definition	Modulus E_i (in terms of λ, μ)	Modulus E_i (in terms of K,G)
Transverse Shear	$\partial u_x/\partial z$	$E^{(1)} = T_{13}/(2S_{13})$	μ	G
Bending	$\partial u_y/\partial z$	$E^{(2)} = T_{23}/(2S_{23})$	≈ 0	≈ 0
Longitudinal Compression	$\partial u_z/\partial z$	$E^{(3)} = T_{33}/S_{33}$	$\frac{4\mu(\lambda + \mu)}{\lambda + 2\mu}$	$\frac{4G(3K + G)}{3K + 4G}$

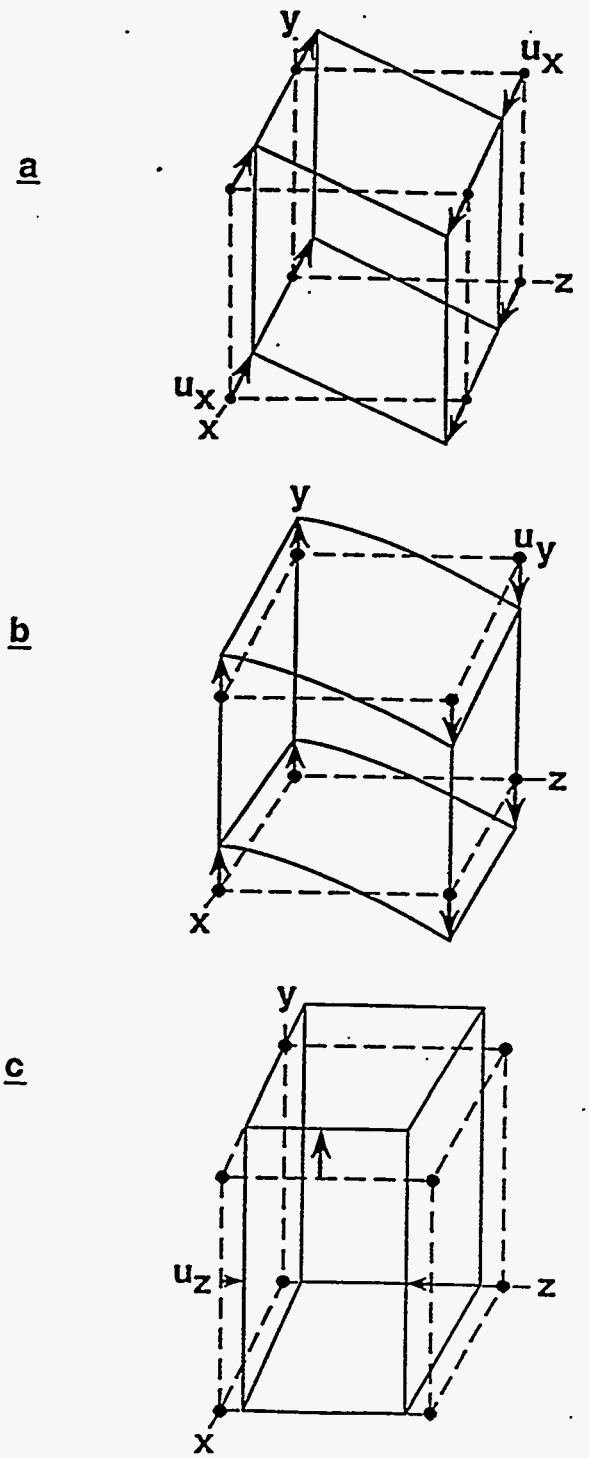

Fig. 4. Strain modes generated in an acoustically thin ($R \ll 1$) film due to sinusoidal variation in the direction of propagation of (a) u_x, (b) u_y, and (c) u_z.

a plane strain arises from this gradient with an associated elongation modulus $E^{(3)} = T_{33}/S_{33}$, given in Table I. For soft, elastic solids having $|K| \gg |G|$, $E^{(3)} \approx 4G$. Thus, while this strain mode is tensile (compressive), the ability of the film to contract (expand) in the surface-normal direction yields an elongation modulus $E^{(3)}$ determined largely by the shear modulus G.

SAW Response from Acoustically Thin Films

Changes in SAW propagation velocity and attenuation are determined by the mechanical impedances at the substrate/film interface resulting from film translational and strain modes (see Appendix C). The impedance associated with each film *translation* is jωρh, and with each *strain mode*is $-j\omega h E^{(i)}/v_o^2$, where $E^{(i)}$ are taken from Table I. Thus, from a perturbation analysis (Appendix C), the change in SAW propagation arising from acoustically thin films, denoted here as Model 1, is:

$$\underline{\text{Model 1}}: \quad \frac{\Delta\gamma}{k_o} = \frac{\Delta\alpha}{k_o} - j\frac{\Delta v}{v_o} = j\omega h \sum_{i=1}^{3} c_i \left(\rho - \frac{E^{(i)}}{v_o^2} \right) \tag{5}$$

where the SAW-film coupling parameter $c_i = v_{io}^2/(4k_oP)$: v_{io} denotes the surface particle velocity (related to surface displacements by $v_{io} = j\omega u_{io}$) in each direction, and P is the SAW power density (power flow per beam width). The c_i parameters, given in Table II for X-propagation in the ST-cut of quartz[28], are determined for SAW propagation in the uncoated substrate and are assumed to be unchanged by the film.

Each displacement component contributes two terms to Eq. 5: one, proportional to ρ, arises from the *kinetic* energy associated with film translation; another, proportional to $E^{(i)}$, arises from the *potential* energy associated with film strains (modes shown in Fig. 4). The kinetic contribution causes a SAW velocity decrease in proportion to film mass per area (ρh)--the mass loading contribution. The relative *kinetic* contribution from each displacement component is proportional to the SAW-film coupling parameter c_i. From Table II, the u_y and u_z displacements make a significant kinetic contribution to SAW propagation, while the u_x contribution is negligible for X-propagation in ST-quartz.

Table II. SAW-Film coupling parameter c_i and phase angles ψ_i for SAW propagation in the X-direction of ST-cut quartz.

Displacement Component	$c_i = v_{io}^2/(4k_o P)$ (x 10^{-7} cm^2-s/g)	ψ_i (deg)
u_x	0.013	90
u_y	1.421	90
u_z	0.615	0

From Eq. 5, the relative importance of each film *strain* mode in perturbing SAW propagation is determined by the product $c_i E^{(i)}$. We note from Tables I and II that *only the u_2 component has both a significant displacement amplitude (c_3) and associated modulus ($E^{(3)}$) to make a significant elastic contribution to SAW propagation.* Thus, for acoustically thin films, one need consider only the strain mode illustrated in Fig. 4c, generating tension and compression in the direction of propagation (with a corresponding expansion and contraction in film thickness) to account for (visco)elastic contributions to velocity and attenuation.

Equating real and imaginary parts of Eq. 5 yields velocity and attenuation changes resulting from the SAW/film interaction. With *elastic* films, the intrinsic elastic moduli are real, resulting in real $E^{(i)}$ and imaginary $\Delta\gamma/k_o$, so that $\Delta\alpha/k_o = 0$. Substituting the $E^{(i)}$ expressions written in terms of the Lame' constants (λ, μ) from Table I into Eq. 5 yields the Tiersten (Wohltjen) formula[14]

$$\frac{\Delta v}{v_o} = -\omega h\left[c_1\left(\rho - \frac{\mu}{v_o^2}\right) + c_2\rho + c_3\left(\rho - \frac{4\mu}{v_o^2}\frac{\lambda+\mu}{\lambda+2\mu}\right)\right] \qquad (6)$$

which gives the SAW velocity change contributed by an acoustically thin (R « 1), elastic ($K'' = G'' = 0$) film.

While Eq. 6 does not apply to *viscoelastic* films, the velocity and attenuation arising from acoustically thin, viscoelastic films can be determined from Eq. 5 by inserting complex moduli (e.g., K and G) into the $E^{(i)}$ expressions. A simplification can be made in Eq. 5 by noting that the bulk modulus in soft, elastic solids is typically much larger than the shear modulus ($|K| \gg |G|$), so that $E^{(3)} \approx 4G$. The velocity and attenuation changes arising from an acoustically thin (R « 1) *viscoelastic* film (written in terms of the commonly reported polymer properties K, G) are then:

$$\frac{\Delta v}{v_o} \cong -\omega h\left(\left(c_1 + c_2 + c_3\right)\rho - \frac{\left(c_1 + 4c_3\right)}{v_o^2}G'\right) \qquad (7a)$$

$$\frac{\Delta\alpha}{k_o} \cong \frac{\omega h}{v_o^2}\left(c_1 + 4c_3\right)G'' \qquad (7b)$$

where c_1 - c_3 are as listed in Table II. The first point of departure from the Tiersten model is that

viscoelastic films cause an *attenuation response* in addition to a velocity response.

Reference to Fig. 3 shows that caution must be exercised in applying Eqs. 5 - 7 to polymer-coated SAW devices. Even polymer films with h « Λ have only a limited range (glassy regime plus part of the transition region) in which they actually behave as *acoustically* thin. In the regime where in-plane gradients dominate and Eqs. 5 - 7 apply, the SAW response depends in a simple way on the intrinsic polymer shear modulus G: for constant ρ, velocity changes correspond to changes in G' ($\Delta G'$) and attenuation changes reflect changes in G'' ($\Delta G''$). (It should be noted that the *additional* SAW response due to *changes* in film properties is evaluated using Eqs. 7 where the terms ρ, G', G'' are replaced with the change terms $\Delta\rho$, $\Delta G'$, and $\Delta G''$.)

If the glass transition is defined as the temperature corresponding to a maximum in the intrinsic shear loss modulus (G''), then Eq. 7b indicates that a peak in $\Delta\alpha/k_o$ signals the glass transition at the SAW operating frequency. However, the rapid decrease in G' that accompanies the glass transition causes all but the thinnest ($h < 20$ nm) films to behave as acoustically thick precisely at this point. As will be shown below, acoustically thick films exhibit attenuation peaks at points *not* coincident with the intrinsic loss maximum, making identification of T_g problematical with a high frequency SAW device.

Strain Modes in Acoustically Thick Films

Neglecting the SAW-induced in-plane gradients for the moment, we focus on a portion of the film that is small in lateral extent compared with the SAW wavelength. As the wave passes a fixed point, the lower surface of the film oscillates laterally in response to the sinusoidal SAW surface displacement (Fig. 5). If the film is acoustically thick ($R \geq 1$), the upper portions of the film tend to lag behind the driven substrate/film interface, inducing strains across the thickness of the film. This *inertial deformation* of the film, resulting in nonuniform displacement across the film (i.e., u_i depend on y) leads to non-zero gradients in the direction *normal* to the film surface (i.e., non-zero $\partial u_i/\partial y$) and generation of S_{i2} strains. Since cross-film gradients arise from inertial deformation, they are strongly dependent upon film properties and operating frequency, as opposed to in-plane gradients that are imposed by wave periodicity. The effect of these cross-film or inertial strains on SAW velocity and attenuation are *not* included in Eqs. 5 - 7.

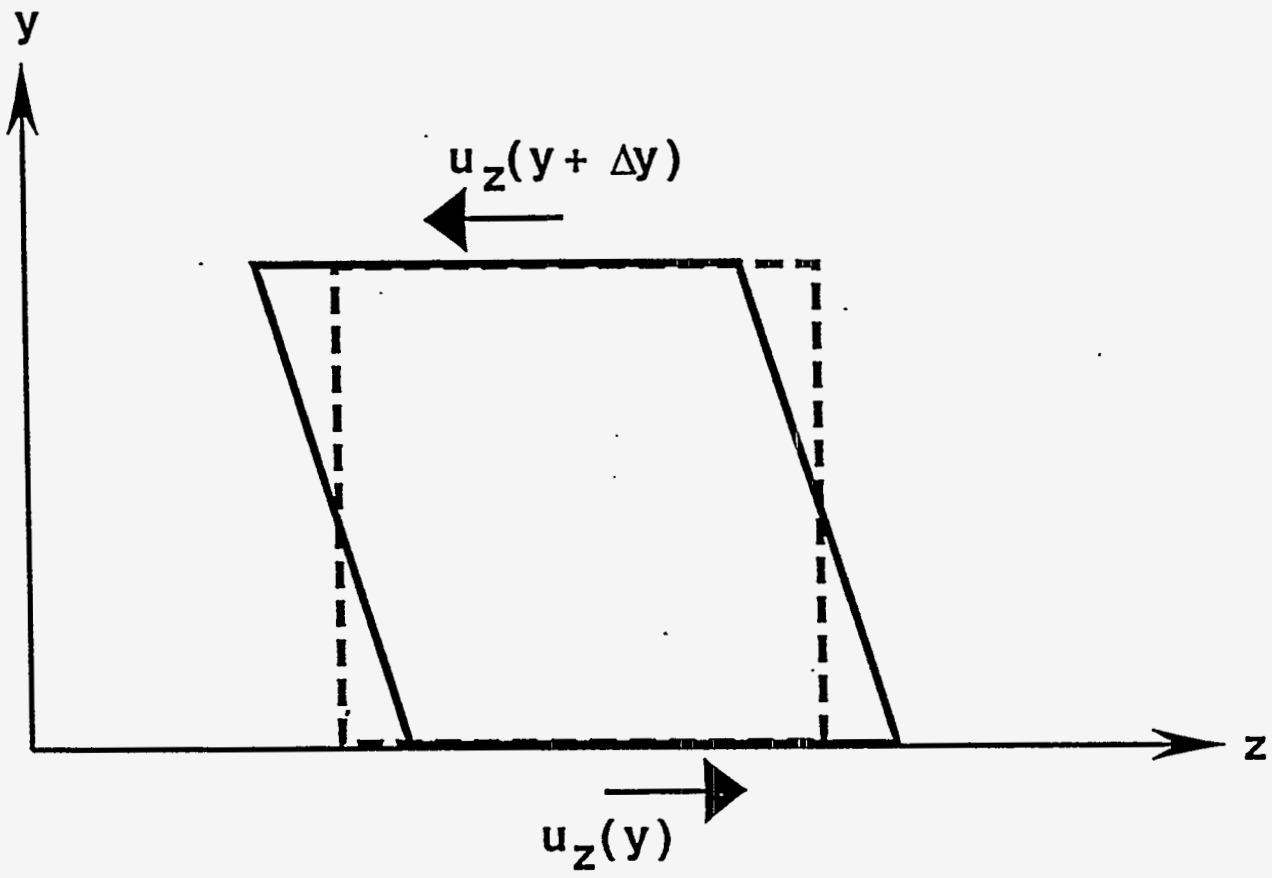

Fig. 5. Inertial lag of the upper film region with respect to the lower "driven" surface leads to a cross-film gradient in u_z, generating shear deformation in the film.

Dynamic Cross-Film Behavior. The displacement in an acoustically thick ($R \geq 1$) film is calculated in Appendix D as:

$$\vec{u}(y,z,t) = e^{j(\omega t - kz)} \sum_{i=1}^{3} u_{io}\, e^{j\psi_i} \left(\frac{\cosh[j\beta_i(y-h)]}{\cosh(j\beta_i h)} \right) \hat{x}_i \tag{8a}$$

where

$$\beta_i = \omega \left(\frac{\rho - E^{(i)}/v_o^2}{M_i} \right)^{\frac{1}{2}} \tag{8b}$$

with $M_1 = M_3 = G$, while $M_2 = K$; ψ_i and $E^{(i)}$ values are as given in Tables I and II. The β_i factors in Eqs. 8 represent propagation constants for waves with polarization direction x_i propagating *across the film* (Fig. 6): β_1 and β_3 are associated with shear wave propagation, while β_2 describes compressional wave propagation. (For a viscoelastic material, characterized by complex bulk and shear moduli, the β_i are complex.) Displacement in the film arises from a superposition of waves generated at the substrate/film interface by the surface displacements u_{io} and radiated into the film (Fig. 6): the surface-normal component u_{yo} generates compressional waves, while the in-plane components (u_{xo}, u_{zo}) generate shear waves. Since $u_{yo} \gg u_{xo}, u_{zo}$ is the dominant source for shear waves.

As indicated in Appendix D, the perturbations to SAW velocity and attenuation caused by the film are related to the mechanical impedances experienced by the surface displacement components in deforming the film. The upper film surface reflects the radiated waves downward so that the mechanical impedance seen at the substrate/film interface is dependent upon the phase shift and attenuation undergone by the waves in propagating across the film. Consequently, a distributed model is used for the film, in which the impedance at the lower film surface depends upon the nature of the *interference* between the waves generated at the lower film surface and those reflected from the upper (film/air) surface.

Film interference for each polarization is dependent upon the acoustic phase shift ϕ_i across

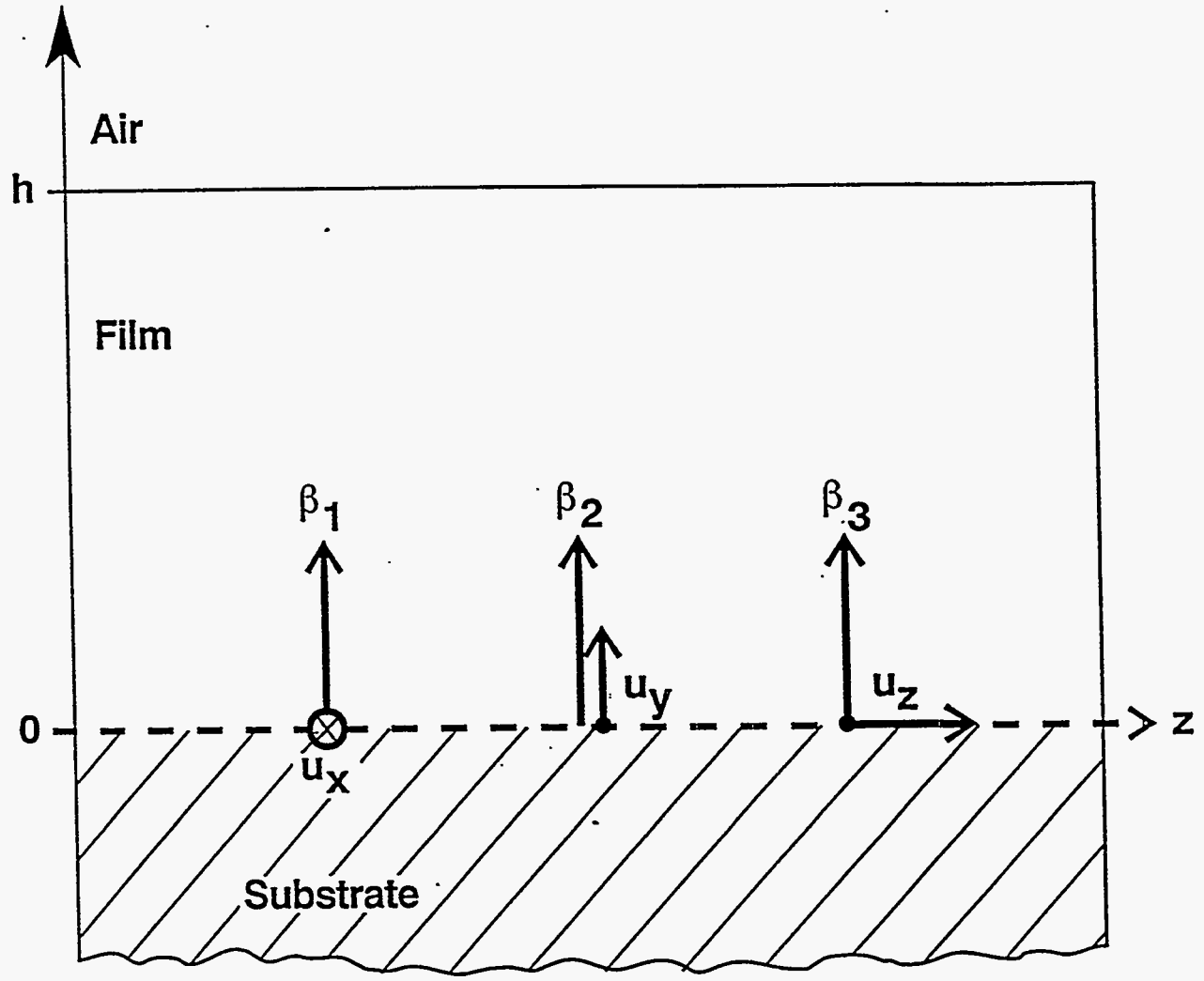

Fig. 6. Displacement in the film is a superposition of waves generated at the substrate/film interface by the surface displacements u_{io} and radiated across the film with propagation factors β_i: the surface-normal component u_{yo} generates compressional waves while the in-plane components (u_{xo}, u_{zo}) generate shear waves.

the film and the attenuation or intrinsic lossiness r_i. The phase shift for each polarization is $\phi_i = Re\{\beta_i h\}$, where $Re\{\ \}$ denotes the real part of the complex expression. For acoustically-thick *elastic* films, $\phi_1 \cong \phi_3 \cong \omega h(\rho/G')^{1/2}$ and $\phi_2 \cong \omega h(\rho/K')^{1/2}$.

Since the magnitude of the bulk modulus K remains in the vicinity of 10^{10} dyne/cm^2 in both glassy and rubbery states, ϕ_2 remains small ($< \pi/2$) for typical polymer thicknesses: $h < 1$ μm. Thus, *polymer films remain acoustically thin with regard to compressive displacement* (u_{yo}) applied to the lower film surface. Consequently, $u_y(y)$ can be regarded as nearly constant across the film so that the surface displacement component u_{yo} simply causes a vertical translation of the film.

Since G' can be as low as 10^7 - 10^8 dyne/cm^2 in rubbery polymer films, with ϕ_1 and ϕ_3 reaching $\pi/2$ for films as thin as 80 nm (at 100 MHz), *films do not remain acoustically thin with regard to shear displacements* applied to the lower film surface. Since $c_3 \gg c_1$, for an x-propagation SAW in ST-cut quartz, the phase shift ϕ_3 associated with the z-polarized shear wave is the most important in determining the response with acoustically thick films:

$$\phi_3 \equiv Re\{\beta_3 h\} \cong \frac{\omega h\left[(a^2 + b^2)^{1/2} + a\right]^{1/2}}{\sqrt{2}\,|G|} \tag{9}$$

with $a = (\rho G' - 4|G|^2/v_o^2)$ and $b = \rho G''$. Eq. 9 allows the critical ϕ_3 phase shift to be calculated in terms of the intrinsic film properties.

The film loss parameter $r_i \equiv -Im(\beta_i)/Re(\beta_i)$ describes the intrinsic lossiness of the film as experienced by the x_i-polarized wave. This parameter, a ratio of power dissipation to energy storage, is analogous to a loss tangent, taking on values between 0 and 1 for all viscoelastic materials: $r_i = 0$ for an elastic film and increases toward 1 for purely viscous films. For the z-polarized shear wave:

$$r_3 \equiv -\frac{Im(\beta_3)}{Re(\beta_3)} \cong \left[\frac{(a^2 + b^2)^{1/2} - a}{(a^2 + b^2)^{1/2} + a}\right]^{\frac{1}{2}} . \tag{10}$$

Fig. 7 shows the shear displacement profile at the point of maximum substrate surface

excursion for various values of the shear wave phase shift ϕ_3 and $r_3 = 0.2$. If the film coating is rigid (e.g., a glassy polymer), $\phi_3 \approx 0$ (curve a) and the entire film moves synchronously with the surface. Since the shear displacement is uniform across the film, no elastic energy is stored or dissipated due to inertial effects. As ϕ_3 increases, the variation in shear displacement across the film increases. In curve b, where $\phi_3 = \pi/4$, the upper film displacement "overshoots" the lower film surface. When the film phase shift reaches $\pi/2$ (curve c), a condition of *film resonance* is reached, causing maximum coupling of acoustic energy from the SAW to the film. As ϕ_3 surpasses $\pi/2$ (curve d), the upper and lower film surfaces go from an in-phase to an out-of-phase condition. This change in film dynamics with ϕ_3 has a profound effect on device response. Similar dynamic behavior occurs with thickness-shear mode resonators coated with polymer films[29].

SAW Response with Acoustically Thick Films

The dynamic film behavior outlined above influences the coupling of acoustic energy from the SAW into the film and hence, the propagation velocity and attenuation. The combined influences of in-plane and surface-normal gradients on SAW velocity and attenuation are calculated in Appendix D. The resulting perturbational formula for the SAW velocity and attenuation changes, applying to either acoustically thin or thick viscoelastic films, and denoted herein as Model 2, is:

$$\underline{\text{Model 2}}: \frac{\Delta\gamma}{k_o} = \frac{\Delta\alpha}{k_o} - j\frac{\Delta v}{v_o} = \sum_{i=1}^{3} \frac{c_i \beta_i M_i}{\omega} \tanh(j\beta_i h) \quad . \tag{11}$$

Calculating the sum in Eq. 11 and equating real and imaginary parts determines $\Delta\alpha/k_o$ and $\Delta v/v_o$ explicitly.

Model Predictions For acoustically thin films, $|\beta_i h| \ll 1$ for i=1, 2, 3, so that $\tanh(j\beta h) \cong j\beta h$, resulting in:

$$\frac{\beta_i M_i}{\omega} \tanh(j\beta_i h) \rightarrow j\omega h \left(\rho - \frac{E^{(i)}}{v_o^2} \right) \quad . \tag{12}$$

Thus, for acoustically thin films, in which surface-normal gradients vanish, Model 2 (Eq. 11) reduces to Model 1 (Eq. 5), as required.

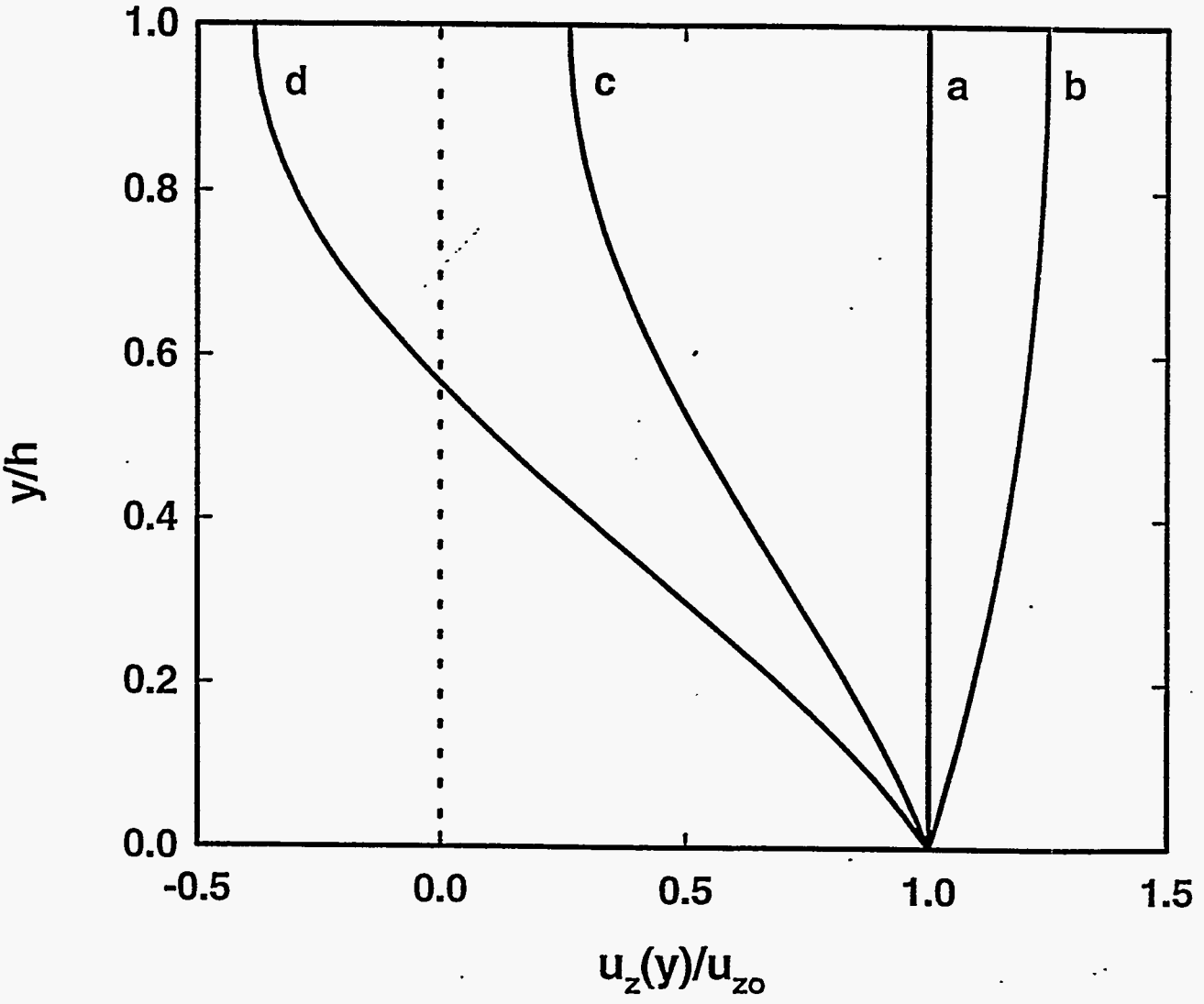

Fig. 7. Shear displacement across an acoustically thick ($R \geq 1$) film arising from inertial deformation for ϕ_3 values (a) 0, (b) $\pi/4$, (c) $\pi/2$, (d) $3\pi/4$.

For acoustically thick, *elastic* films, β_i are real and $\tanh(j\beta_i h) = j \tan(\phi_i)$. In this case, the sum in Eq. 11 is imaginary, so that $\Delta\alpha/k_o = 0$, as expected. The behavior of $\Delta v/v$ is more interesting: when $\phi_i = n\pi/2$ (n = 1,3,5...), then $\tan(\phi_i)$ "blows up" causing a large negative excursion in $\Delta v/v_o$ for $\phi_i = n\pi/2^-$ and a large positive excursion for $\phi_i = n\pi/2^+$. This is a consequence of *film resonance*, occurring when the shear stresses applied to the lower film surface interfere constructively with those reflected from the upper film surface. Concurrently, the shear particle velocities are interfering destructively, so that the surface mechanical impedance Z_i (the ratio of stress to particle velocity) becomes infinite. Of course, the films of interest in this study are viscoelastic, exhibiting complex β_i; this leads to imperfect interference so that $\Delta v/v_o$ and $\Delta\alpha/k_o$ remain finite. Nonetheless, dramatic responses are observed whenever film resonances are encountered.

As described previously, the compressional wave phase shift $\phi_2 \ll \pi/2$ in all polymer states, so *compressional wave resonances should not be observed.* The surface mechanical impedance experienced by the u_y component reduces to $j\omega\rho h$; thus, only the *mass* of the film is sensed by the surface-normal component.

The shear wave phase shifts ϕ_1 and ϕ_3 may easily reach $\pi/2$ (for $h \geq 0.25$ μm at 100 MHz) and elicit film resonant responses. Since $c_3 \gg c_1$ when an ST-cut quartz substrate is used, *the z-polarized shear wave resonance dominates the SAW viscoelastic response with an acoustically thick film.* Thus, the effect of shear wave film interference on the SAW response is described by the $\tanh(j\beta_3 h)$ term in Eq. 11. Fig. 8 shows the contributions of this term to SAW velocity and attenuation vs. ϕ_3 for several values of the film loss parameter r. The parameter ϕ may be considered a *normalized film thickness.* The SAW velocity decreases linearly with film thickness for $\phi_3 \leq 0.2\pi$ at a rate consistent with the thin-film prediction (dashed line calculated from Eq. 6, independent of film loss r_3). As ϕ_3 surpasses 0.2π, an *excess* velocity response arises due to shear-wave interference effects. The size of this excess response varies inversely with the film loss parameter r_3. For $\phi \ll 0.5\pi$, SAW attenuation increases linearly with film thickness and is proportional to G'', as predicted by Eq. 7b.

In Fig. 8, a pronounced response occurs at $\phi_3 = \pi/2$: attenuation goes through a maximum

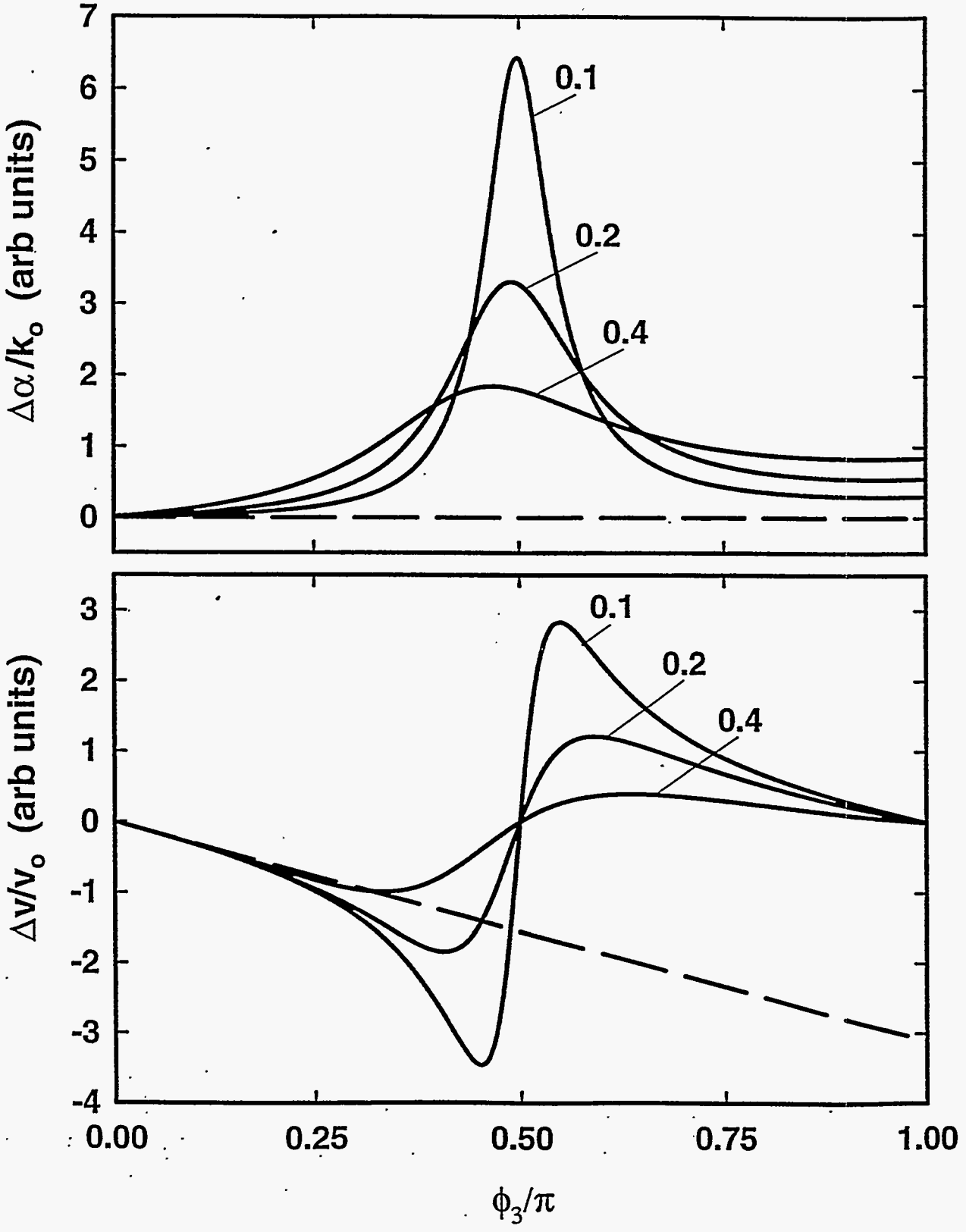

Fig. 8. The contributions to SAW velocity and attenuation vs. the shear wave phase shift ϕ_3 for several values of the film loss parameter r_3. The dashed line is predicted from the Tiersten[14] (Wohltjen) formula (Eq. 6).

while velocity undergoes an upward transition. These responses are easily confused with the intrinsic relaxation response occurring at the glass transition--a monotonic decrease in G', and a peak in G''. However, a device with an acoustically thin film, whose response tracks these intrinsic film changes, should exhibit a peak in attenuation coincident with a *velocity decrease* (rather than increase). The responses in Fig. 8 are due to shear-wave interference effects in the film. A shear-wave *resonant response* at $\phi_3 = \pi/2$ is most pronounced with low-loss films ($r_3 \ll 1$) and becomes damped as r_3 approaches unity. Off-resonant attenuation increases *proportionally* with film loss, while resonant attenuation is *inversely* dependent upon film loss. In the extreme case of a purely elastic film, a delta function attenuation response is predicted: attenuation is zero for $\phi_3 \neq \pi/2$, but becomes infinite for $\phi_3 = \pi/2$.

The SAW resonant response predicted vs. ϕ_3 can be related to the dynamic film behavior outlined in Fig. 7. As ϕ_3 passes $\pi/2$, film motion at the upper surface goes from an in-phase to an out-of-phase condition (with respect to the lower film surface). This coincides with the sigmoidal upward transition predicted in the SAW velocity response. This phase transition results in a smaller particle excursion in the upper regions of the film, diminishing the kinetic contribution to velocity response. That is, film mass loading is diminished as ϕ_3 exceeds $\pi/2$.

The resonant response at $\phi_3 = \pi/2$ is predicted to recur at $3\pi/2$, $5\pi/2$, etc., constituting *harmonics* of the fundamental film resonance. Since the resonance damping varies as $r_3\phi_3$, however, the harmonic resonant responses become less pronounced. Ballantine[30] has reported observing harmonic film resonances up to n = 9; however, results presented in the Results and Discussion section of this paper cast doubt on this interpretation.

Parametric Representation Frequently, the representation of velocity and attenuation perturbations is simplified by using a parametric representation in which attenuation changes are plotted vs. velocity changes (or *vice versa*) while some independent parameter is varied[25]. Since velocity and attenuation were shown (Appendices C and D) to be related to the components of a complex surface mechanical impedance, this representation is equivalent to a *Nyquist*[31] or *Cole-Cole*[32] plot in which the imaginary component of impedance is plotted vs. the real component (frequency is typically the varying parameter). Fig. 9 shows a parametric plot of attenuation vs. velocity contributions arising from the $\tanh(j\beta_3 h)$ term of Eq. 11 as ϕ varies from 0 to π for several values of the film loss

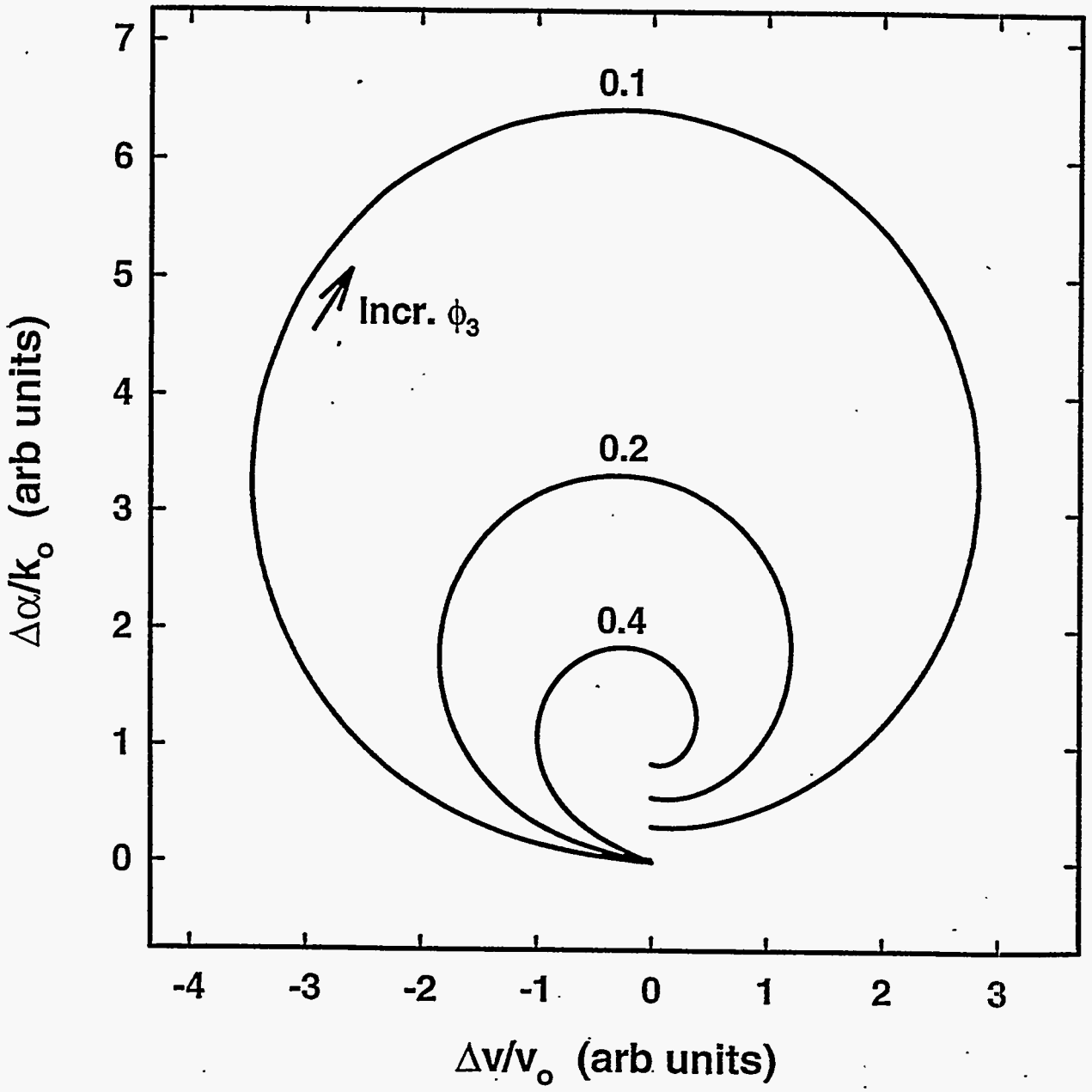

Fig. 9. Parametric plot of attenuation changes vs. velocity changes as ϕ_3 varies from 0 to π for several values of the film loss parameter r_3.

parameter r_3. When only ϕ_3 is varied (r_3 fixed), the locus of ($\Delta v/v_o$, $\Delta\alpha/k_o$) points generated by film resonance forms a spiral. The curvature and pitch of the spiral are proportional to r_3; a near-circle is formed when r_3 is small. The utility of the parametric plot in comparing data obtained by varying film parameters in different ways is illustrated in the Results and Discussion section.

Dependence of Film Properties on Temperature and Vapor Absorption

A number of film parameters must be considered in modeling the response of polymer-coated SAW devices to temperature changes or vapor absorption. These include changes in: (1) shear modulus G (most important), (2) bulk modulus K, (3) film thickness h, and (4) mass density ρ. In addition, the temperature behavior of the substrate must be included.

Fig. 10 illustrates how a typical polymer's viscoelastic properties, i.e., storage and loss components of the bulk[33] and shear[34] moduli, vary with the apparent probe frequency ω' at fixed temperature T_o. At high probe frequencies, the storage components (K', G') are maximum and the polymer is in the glassy state. As ω' decreases, a polymer *relaxation* or *glass transition* is exhibited by the intrinsic elastic properties: K' and G' decrease monotonically, while K'' and G'' go through a maximum. For $\omega' \leq 2$, the polymer is in the rubbery state. The small changes that occur in K' in comparison with G', and the fact that SAW response is inherently less sensitive to K than G in the transition regime, results in SAW responses arising largely from changes in G rather than changes in K.

From the time-temperature superposition principle[35], changes in the viscoelastic properties with temperature or vapor absorption can be expressed as a translation a_T in the polymer relaxation time or the apparent probe frequency ω':

$$\log(\omega') = \log(\omega) + \log(a_T) \quad . \tag{13}$$

Thus, the curves of Fig. 10 may be considered "master curves" that can be used (*vide infra*) to describe the moduli as either a function of frequency, temperature, or vapor absorption.

In addition to causing a horizontal translation in ω', temperature changes lead to a slight vertical translation[33] in modulus values due to (1) the inherent modulus dependence on absolute

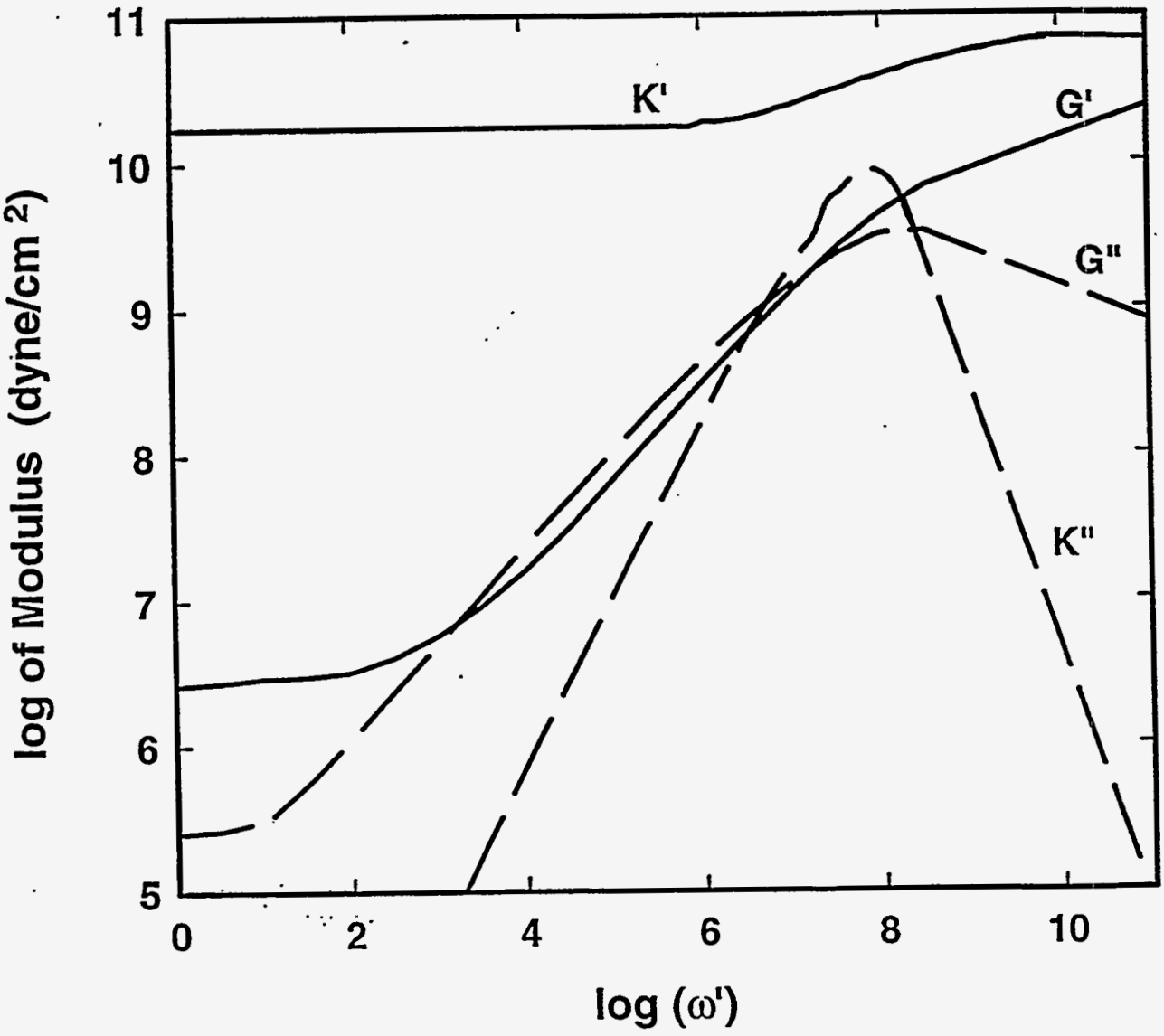

Fig. 10. Storage (′) and loss (″) components of the bulk[33] (*K*) and shear[34] (*G*) elastic moduli for polyisobutylene (avg. molecular weight = 1.56×10^6) vs. log(ω′).

temperature, and (2) changes in polymer chain density. (Film density is inversely related to film thickness h.) To account for these effects, moduli obtained by translation from reference (h_o,T_o) to (h,T) must be multiplied by the factor $(h_oT)/(hT_o)$.

We now introduce a model in which the shift factor a_T is expressed in terms of a polymer free volume F, analogous to the derivation of the WLF equation[36], but modified to include the effects of vapor absorption. Free volume is volume *not* occupied by polymer molecules, present as voids of molecular dimension, that enhances polymer chain segmental mobility. The shift factor a_T is given by the generalized Doolittle equation[37]:

$$\log(a_T) = \frac{B}{2.303}\left(\frac{1}{F} - \frac{1}{F_o}\right) \tag{14}$$

where B is a constant (taken as unity); F is the polymer free volume at any temperature or vapor concentration (T,C), while F_o is the free volume of the *pure* $(C = 0)$ polymer at some reference temperature $(T_o,0)$. We develop this argument in two steps: first, the effects of temperature in the absence of vapor and, second, the additional effects of plasticization and swelling of the polymer film by the vapor.

Temperature Response As polymer temperature increases above the low-frequency glass transition temperature $T_g^{(0)}$, polymer volume expands nearly linearly due to the creation of additional free volume. Due to mechanical constraint in the plane of the film by the substrate, however, volume expansion of the film leads to a combination of increased film thickness and static in-plane compressive stress. The parameter $\xi = 3K'/(3K' + 4G')$, given by Bartley and Dominguez[38], describes the extent to which free volume addition is converted to changes in film thickness. For rubbery films, $K' \gg G'$, so that $\xi \cong 1$ and film expansion accounts for all free volume addition. For glassy films, $K' \approx G'$, so that $\xi < 1$ and free volume accrual is diminished by generation of in-plane compressive stresses. When operating at temperatures above $T_g^{(0)}$, however, the film is rubbery with regard to static stresses (but may still be in the glassy regime at the SAW frequency). Therefore, setting $\xi \equiv 1$ is reasonable, and as demonstrated below, gives an acceptable fit to the data.

For temperatures above $T_g^{(0)}$, the change in free volume with temperature varies as[20]

$$F = F_o + \alpha_f(T - T_o) \tag{15}$$

where F_o is the free volume at the reference temperature[39] T_o and α_f is the polymer (volume) thermal expansion coefficient.

Substituting Eq. 15 into Eqs. 13 and 14 gives the translation in ω', determining the rate of film softening with temperature. Increases in free volume cause a decrease in ω', leading to changes in K and G determined from the "master curves" of Fig. 10. The most pronounced effect is a glass-to-rubber transition in polymer properties, signalled by a rapid decrease in K' and G'.

The film thickness h changes due to thermal expansion:

$$h(T) = h_o\left[1 + \alpha_f(T - T_o)\right] \tag{16}$$

where h_o is the film thickness at the reference temperature T_o. Since the total mass of the film ($h\rho$) is conserved, thermal expansion causes a decrease in film mass density (ρ):

$$\rho(T) = \frac{\rho_o h_o}{h(T)} = \frac{\rho_o}{1 + \alpha_f(T - T_o)} \tag{17}$$

Vapor Response The absorption of vapor molecules, presumed to be of low molecular weight in comparison with the polymer and molecularly dispersed, causes dilution of the polymer. The diluent molecules lower the effective viscosity and reduce T_g and $T_g^{(0)}$. The effect of the diluent on polymer viscoelastic properties at fixed temperature may be thought to arise from the addition of free volume, in proportion to the volume fraction of diluent[20]:

$$F(T, V_1) = F(T) + \chi V_1 \tag{18}$$

where F(T) is the free volume of the pure polymer (without diluent as in Eq. 15), χ is an empirically-determined plasticizing parameter[20], and V_1 is the volume fraction of absorbed vapor: $V_1 = CV/(1 + CV)$, where C is the concentration (mole sorbed vapor/ml of polymer) and V is the specific volume (ml/mole) of absorbed vapor.

The effect of vapor absorption on polymer elastic properties is determined from Eqs. 13, 14,

and 18. As free volume increases with concentration C, the translation factor a_T increases; this leads to a decrease in K and G, according to the master curves of Fig. 10.

Film thickness and density vary with the concentration of absorbed species as:

$$h(C) = h_o(1 + CV) \tag{19a}$$

$$\rho(C) = \frac{\rho_o + Cm}{1 + CV} \tag{19b}$$

where ρ_o is the pure polymer density (at C = 0) and m is the specific mass (g/mole) of the absorbed species.

Combining Eqs. 14, 15, and 18 gives an equation for the shift factor a_T, analogous to the WLF equation, but including the effects of both temperature changes and vapor absorption:

$$\log(a_T) = -\frac{B}{2.303 F_o}\left(\frac{\alpha_f(T - T_o) + \chi V_1}{F_o + \alpha_f(T - T_o) + \chi V_1}\right) . \tag{20}$$

The free volume treatment above indicates the interchangability of temperature and vapor absorption in determining film elastic properties[12,40].

EXPERIMENTAL SECTION

The experiments consist of measuring the response of polymer-coated SAW devices during temperature changes and during vapor absorption by the polymer.

SAW Devices. The SAW devices used in this study consist of an ST-cut quartz substrate with two photolithographically defined Cr/Au (30/200 nm) transducers separated by a path length (transducer center separation) of 7.2 mm. The transducers each consist of 50 finger-pairs of interdigitated electrodes, with periodicity $\Lambda = 32$ μm (8 μm lines and spaces) for a center frequency of 97 MHz. Devices were bonded into flatpacks; electrical connections were made between flatpack feedthroughs and transducer bonding pads with ultrasonically bonded 75 μm Au wires.

Electronic Instrumentation. Due to the large attenuations encountered in these studies, the two-port oscillator circuit normally used to instrument a SAW sensor would not sustain oscillation over all experimental conditions. Thus, the device was instrumented in a phase-lock-loop configuration: a signal generator (Hewlett-Packard 8656B) input a signal to the input transducer (output terminated in 50Ω) while a vector voltmeter (Hewlett-Packard 8508A) monitored changes in amplitude and phase between input and output ports. A computer monitored these vector voltmeter outputs, controlling the signal generator frequency to maintain constant phase between input and output. Changes in SAW velocity were determined from the changes in frequency required to maintain constant phase. When the coating covers the entire SAW propagation path, and the external (electrical) phase shift is small compared with the internal (acoustic) phase shift, then $\Delta f/f_o \cong \Delta v/v_o$. Changes in SAW attenuation $\Delta\alpha$ were determined from the changes in signal amplitude (ΔL, dB) measured between input and output ports: $\Delta\alpha/k_o = \Delta L/(54.6 N_\Lambda)$, where k is the acoustic wavenumber ($k_o = 2\pi/\Lambda = 1960$ cm^{-1}) and N_Λ is the acoustic path length (225 wavelengths).

Polymer Coating. Polyisobutylene (PIB) (Aldrich: mw = 380,000, density 0.92 g/cm^3) coatings were prepared by spin casting at 2000 rpm for 30 sec from solutions in chloroform. The solution concentration was varied from 2.0% to 3.5% (by weight) to vary the film thickness of the resulting coatings. Film thickness measurements were attempted by profilometry (Dektak 3030). However, the softness of the films resulted in stylus penetration into the film and erroneously low readings. Therefore, film thicknesses were obtained by measuring changes in transducer center frequency for chilled SAW devices (-10°C) before and after film deposition. SAW velocity changes were

determined from the changes in the transducer center frequency, measured using an HP8751A network analyzer, from which film thickness was estimated. For films chilled into the glassy regime and behaving as acoustically thin, Eq. 7a relates $\Delta v/v_o$ to film thickness h. Using $G' = 10^{10}$ dyne/cm^2 and $\rho = 0.92$ g/cm^3 for PIB (-10° C, 97 MHz), mass loading accounts for 88% of the velocity shift, while film elasticity accounts for 12%.

Temperature Measurement. Temperature ramps were obtained by placing the test case containing the SAW device in an environmental chamber whose temperature was under computer control. A dry N_2 purge was maintained over the device during the four hour temperature ramps.

Vapor Measurement. Vapor isotherms were obtained using a test case with gas inlet and outlet ports and passing a gas stream across the device maintained at constant temperature (20°C). A computer-controlled vapor test system varied the vapor concentration by varying the relative flow rates of a nitrogen carrier stream saturated with the vapor (by passage through a bubbler) with a nitrogen mix-down stream[41]. The vapor partial pressure p was varied from 0 to 97% of the saturation vapor pressure (p_o) at 20°C and then back to 0 over a 2 hr interval.

To determine the concentration of vapor absorbed into the polymer film, an identical PIB film was deposited on a 5 MHz quartz crystal microbalance (QCM, Maxtek Inc., Torrance, CA). The coated QCM was placed in the gas stream with the coated SAW device and changes in its resonant frequency were monitored during the vapor isotherm. Due to its much lower frequency, the 5 MHz QCM responds as a nearly ideal gravimetric detector for this range of film thicknesses[29]. Thus, changes in resonant frequency indicated the mass of vapor absorbed into the film, from which absorbed vapor concentration was determined.

Calculations. SAW velocity and attenuation responses were calculated from Model 1 (Eq. 5) and Model 2 (Eq. 11), implemented as a computer program for IBM-compatible computers written in HT Basic (TransEra, Provo, UT). This language conveniently handles complex variables and functions of complex variables, e.g., $\tanh(j\beta_i h)$ in Eq. 11.

RESULTS AND DISCUSSION

Temperature Response

PIB-Coated SAW Temperature Measurements. Fig. 11 shows velocity and attenuation measurements (points[42]) vs. temperature for an uncoated 97 MHz SAW device and one coated with a 0.73 μm PIB film. Velocity and attenuation changes are referenced to values measured at the lowest temperature with the film. As temperature increases, the quartz substrate contributes a slight increase in attenuation and a significant change in wave velocity (velocity varies parabolically with temperature in ST-cut quartz with a turnover temperature of 20°C[43]). Since the coated device response is due to both the film and substrate, the *difference* in responses is attributable to the film overlay. Below 80°C, the film coating causes attenuation to increase and velocity to decrease more rapidly with temperature than for the uncoated device; this is due to changes occurring in the intrinsic polymer properties (G, K, ρ) as well as film swelling (h). At high temperatures, the response exhibits the characteristic signature for a resonance: a peak in attenuation along with a sigmoidal increase in velocity. This response is very similar to that calculated vs. ϕ_3 in Fig. 8 (for $r_3 = 0.2$), suggesting the shear wave generated by u_z is resonating across the film thickness.

Fig. 11 also shows responses calculated from Model 1 (dashed line) and Model 2 (solid line) using temperature-dependent film parameters and adding in the measured substrate contributions. The components of G and K were determined from the master curves of Fig. 10; ω' values were determined from Eqs. 13 - 15 using the film parameters (T_o, F_o, α_f) given in Table III. The temperature-dependent film thickness $h(T)$ and density $\rho(T)$ were calculated from Eqs. 16 and 17 using α_f and ρ_0 values from Table III and $h_0 = 0.73$ μm. Model 1 accounts for only in-plane displacement gradients (acoustically thin assumption), while Model 2 includes both in-plane and cross-film gradients (thin or thick). From Eq. 4, $R = 1$ at 55°C, indicating the transition from acoustically thin ($T < 55$°C) to acoustically thick ($T > 55$°C) behavior. This transition point is seen to be a good estimate of where Model 1 breaks down. In the acoustically thin regime, Models 1 and 2 are both valid and adequately fit the attenuation and velocity changes with temperature. The Tiersten[14] formula, Eq. 6, describes $\Delta v/v_o$ in this regime but does not account for the attenuation observed. The peak in $\Delta\alpha/k_o$ at 40°C predicted by Model 1 and followed by the data below 40°C is due to a peak in the intrinsic loss modulus G'' (Fig. 10).

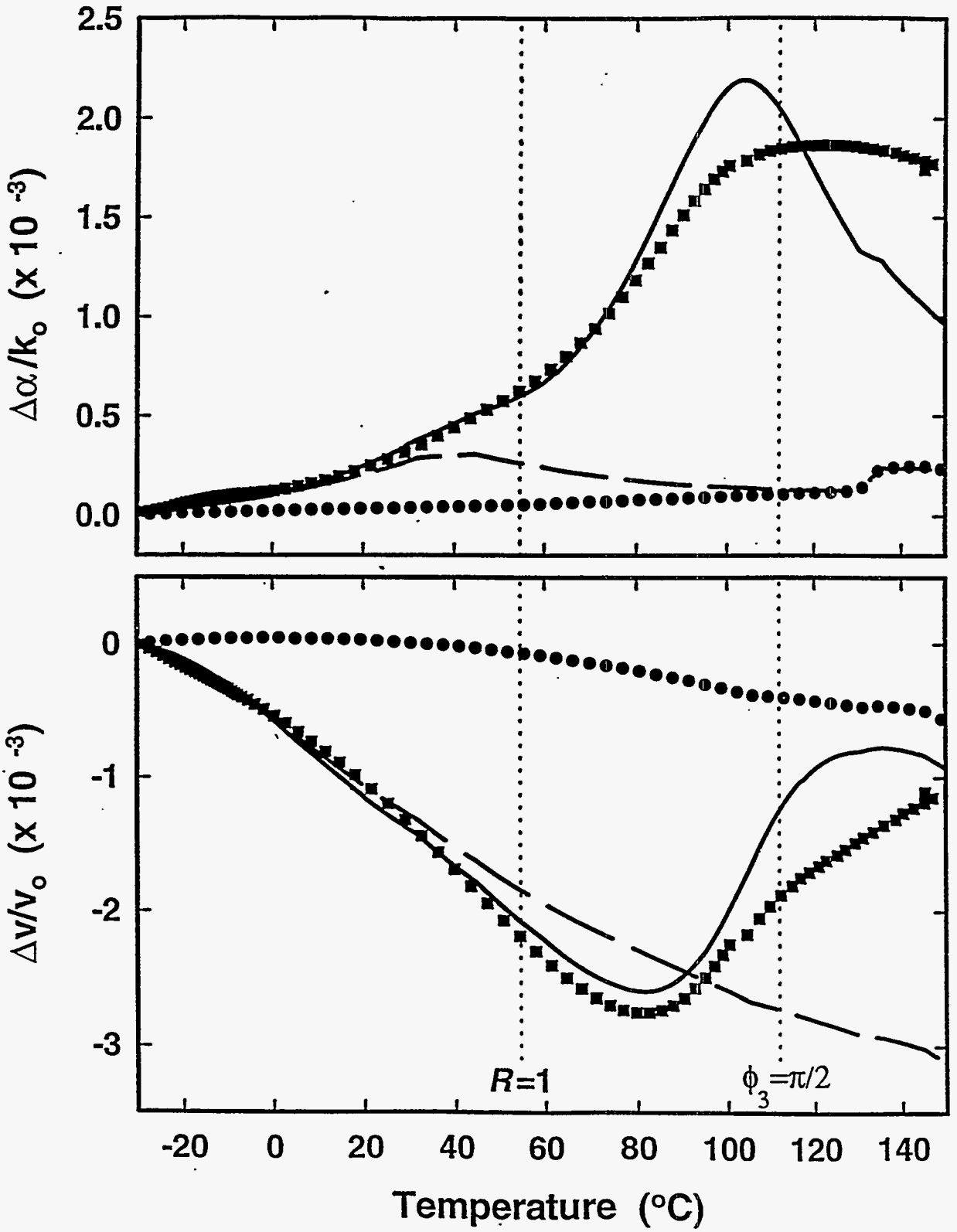

Fig. 11. Velocity and attenuation measured (points) and calculated (lines) vs. temperature for a 97 MHz SAW device: (●) uncoated, and (■) coated with a 0.73 μm-thick polyisobutylene film. Vertical lines indicate transition point (R = 1) between acoustically thin and thick

Table III. Model parameters for polyisobutylene[48].

Parameter	Value
$T_g^{(0)}$	205°K
T_o	293°K
F_o	0.050
α_f	2.5×10^{-4} /°C
ρ_o	0.92 g/cm^3

At temperatures above 55°C the film behaves as acoustically thick and only Model 2 is expected to apply. The Model 2 predictions--an attenuation peak at 104°C and the upturn in velocity beginning at 80°C--are in substantially better agreement with the data than Model 1 predictions. The temperature is indicated in Fig. 11 at which $\phi_3 = \pi/2$ in the responses calculated from Model 2. This marks the center of film resonance: an *inflection* in the sigmoidal velocity response nearly coincident with an attenuation peak. The data and Model 2 predictions show that the intrinsic loss peak (G'') at 40°C is masked by the film resonance centered at 112 C. Thus, *glass transitions cannot be observed unless the film resonance is far enough removed from the glass transition.* Since G' decreases rapidly near T_g, however, film resonance tends to occur in the vicinity of T_g unless the product of frequency and film thickness is small enough to ensure that R remains much less than 1. For high frequency SAW devices, only extremely thin films avoid this problem.

An alternative device, the flexural plate wave (FPW) device[44], has the same (or greater) inherent sensitivity to film properties, while operating at a much lower frequency. Because of the lower frequency, similar film thicknesses on the two devices result in a much lower R-value on the FPW device. For example, measurements on a 1.3 μm PIB film at 5 MHz gave R-values below 0.42 even at the maximum temperature of 100°C. Thus, the T_g at 12 C could be observed in this case without inducing film resonance.

Film Thickness Effects. Fig. 12 shows velocity and attenuation measurements (points) made on 97 MHz SAW devices coated with several thicknesses of PIB. The velocity and attenuation shifts are referenced to the uncoated device. Responses calculated from Model 2 are also shown (lines), using the temperature-dependent values of G, K, ρ, and h described previously and adding in measured substrate contributions. At a sufficiently low temperature for which $R \ll 1$, the velocity offset is proportional to film thickness--due mainly to mass loading by the film. The attenuation curves in Fig. 12 do *not* exhibit a significant offset due to film addition. This is because film-induced attenuation vanishes at low temperatures, due both to a decrease in inertial film strain that occurs as G' and K' increase and diminished intrinsic polymer lossiness (smaller G'' and K'').

It is significant to note in Fig. 12 that the temperature at which attenuation is maximum and

Table IV. Estimates of resonance temperature and maximum $\Delta\alpha/k_o$ vs. polyisobutylene film thickness for 97 MHz SAW devices.

Film Thickness (μm)	Resonance Temperature (°C)	Maximum $\Delta\alpha/k_o$ ($\times 10^{-3}$)
0.44	>120	--
0.73	103	2.25
1.18	74	3.75
1.43	64	4.82

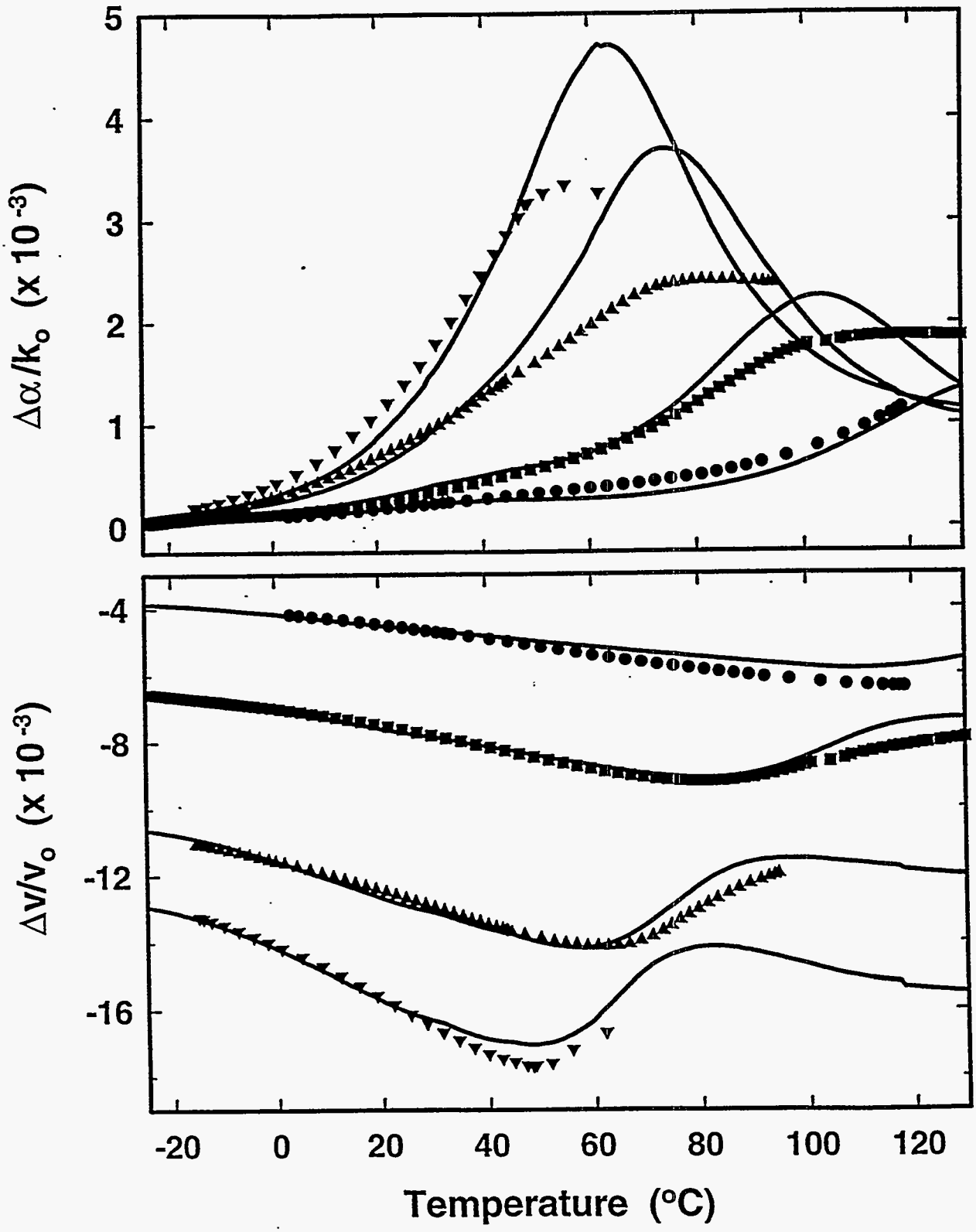

Fig. 12. Velocity and attenuation changes measured (points) and calculated (Model 2, lines) vs. temperature for 97 MHz SAW devices coated with polyisobutylene films of thickness: (●) 0.44, (■) 0.73, (▲) 1.18, (▼) 1.43 μm.

velocity makes its sigmoidal excursion varies inversely with film thickness. Table IV lists the film thicknesses and estimated temperatures where maximum attenuation occurs. These temperatures do *not* coincide with the polymer glass transition temperature T_g of 40°C (where G'' is maximum) at 97 MHz. This argues strongly that the characteristic responses are *not* due simply to changes in the intrinsic film properties, as Martin and Frye[12] originally proposed to explain data exhibiting trends similar to Fig. 12, but are due to thickness-dependent *film resonance effects*. The fact that the resonant temperature depends on film thickness can be understood most easily by considering an elastic film, for which $\phi_3 \cong \omega h(\rho/G')^{1/2}$. Since the fundamental film resonance occurs when $\phi_3 = \pi/2$, $G' = \rho(4fh)^2$ at film resonance. For thicker films, resonance occurs at a larger value of G', achieved at a lower temperature. The measured and calculated responses of Fig. 12 also indicate that the resonant contribution to the velocity and attenuation responses increases proportionally with film thickness.

The measured attenuation peaks shown in Fig. 12 only attain about 2/3 of the calculated attenuation peak heights. This may be due to nonuniformities in film thickness: calculations indicate that thickness variations diminish resonant film interference, analogous to having a higher r_3 value, leading to a smaller attenuation peak.

Vapor Response

PIB-Coated SAW Vapor Measurement. Fig. 13 shows velocity and attenuation responses measured (points) vs. film concentration as pentane and trichloroethylene were absorbed by a 0.70 μm-thick PIB film. Film concentrations were determined from the mass changes recorded in an identical film on a quartz crystal microbalance (QCM) placed in the same vapor stream. The occurrence of an attenuation peak coincident with an upward sigmoidal velocity change indicates that a shear mode film resonance is occurring. The resonance arises in Fig. 13 as vapor molecules plasticize the polymer, decreasing $|G|$, and causing ϕ_3 to pass through $\pi/2$.

The solid lines in Fig. 13 are absorption responses calculated from Model 2. Tables III and V list the PIB and solvent parameters, respectively, used in Eqs. 13, 19, and 20 to calculate concentration-dependent values for G, K, ρ, and h. The solvent specific volumes (V) are estimated as $V = m/\delta$, where m is the solvent specific mass and δ is the liquid density[45]. Accounting for changes in film properties arising from vapor absorption yields calculated responses (Fig. 13, lines)

in reasonable agreement with the measured data. We note that the same plasticizing parameter (χ) was used in calculating both pentane and TCE responses.

At low concentrations, where the film is acoustically thin ($R \ll 1$), a nearly linear $\Delta v/v_o$ response is observed in Fig. 13 vs. absorbed species concentration. The absorption response may be thought of as a superposition of a mass response (proportional to Cm) and a plasticizing response (determined by CV). The plasticizing response is that shown in Fig. 8 and observed during temperature cycling (Figs. 11 and 12). The mass response due to vapor absorption (when $R \ll 1$) can be determined from Eq. 7a, assuming G' and G'' are fixed (no plasticizing effect):

$$\frac{\Delta v}{v_o} = -(c_1 + c_2 + c_3)\omega C m h_o \quad . \tag{21}$$

The mass contribution to $\Delta v/v_o$ from pentane and trichloroethylene, calculated from Eq. 21, is shown in Fig. 13 as dashed lines. The vertical displacement between curves is due to the mass difference (m, Table V) between species. The mass loading contribution accounts for only 40% of the measured (low concentration) $\Delta v/v_o$ response for pentane and 67% for TCE. The remainder of the response is due to film plasticization by the absorbed vapor molecules. This is consistent with a comparison of SAW and chromatography measurements by Grate[21] that indicated that the mass response was a small fraction (25%) of the total $\Delta v/v_o$ response. As the density (m/V) of absorbed species increases, the larger mass contribution relative to the plasticizing contribution results in Eq. 21 predicting the total response more accurately (for $R \ll 1$).

At high vapor concentrations, film plasticization due to acquired solvent volume causes the film to behave as acoustically thick. (TCE exhibits greater solubility than pentane: a 97% saturated vapor ambient at 20°C results in a solvent fraction (V_1 of 0.28 for pentane and 0.38 for TCE.) Film resonance occurs when the solvent plasticization causes ϕ_3 to reach $\pi/2$. Since this occurs at a fixed value of solvent volume fraction V_1 the larger specific volume V of pentane causes the resonant response to occur at a lower concentration than for trichloroethylene.

Film Thickness Effects. Fig. 14 shows velocity and attenuation responses measured vs. the partial (gas phase) pressure of n-pentane for SAW devices coated with several different thicknesses of PIB.

Table V. Model parameters for vapors absorbed by polyisobutylene.

Species	Mass, *m* (g/mole)	Volume, *V* (ml/mole)	Density, δ (g/cm^3)	χ (°C)
n-pentane	72.2	115.2	0.63	0.083
trichloro-ethylene	131.4	89.7	1.46	

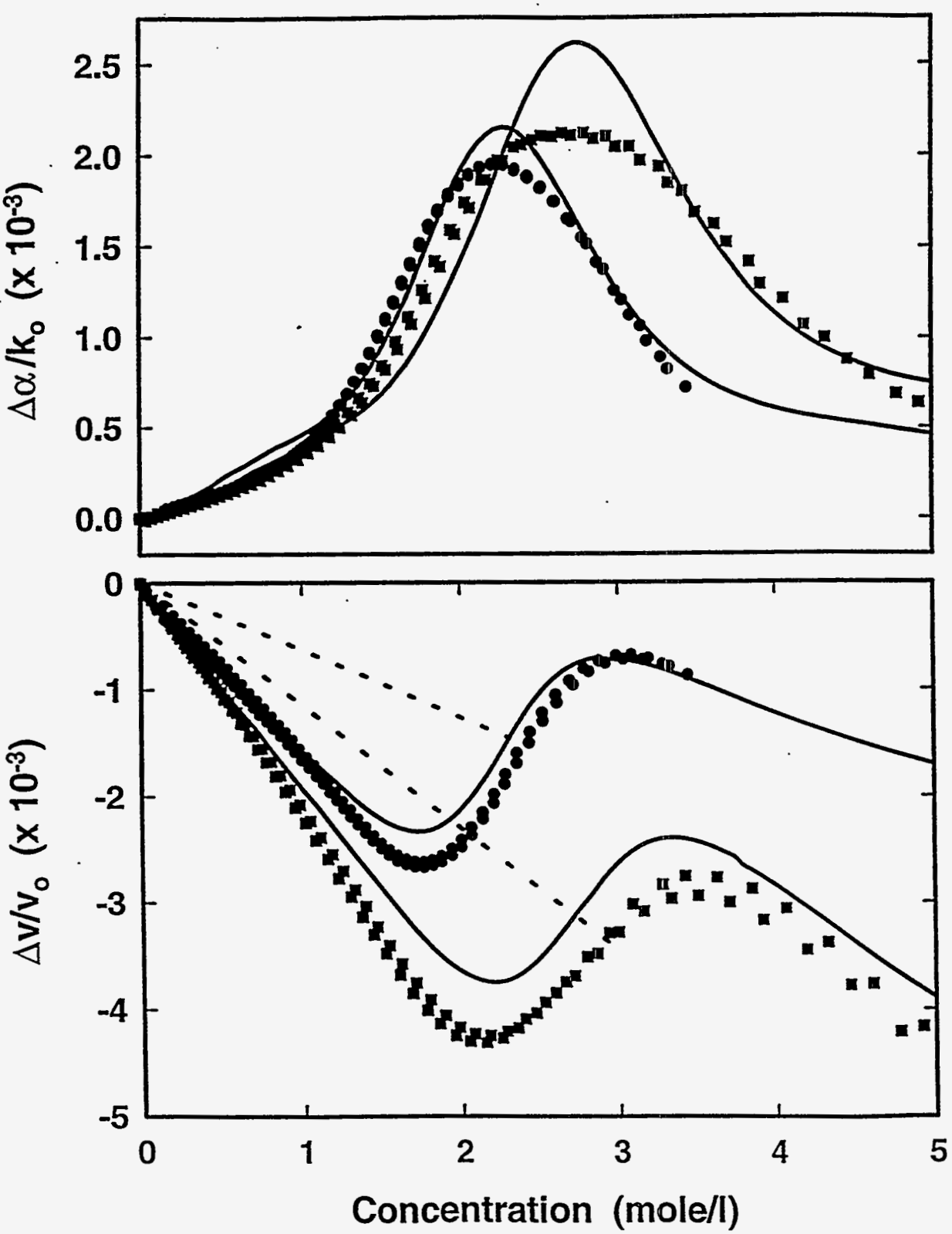

Fig. 13. Velocity and attenuation changes measured (points) and calculated (Model 2, solid lines; mass-loading contribution, Eq. 21, dashed lines) vs. absorbed (●) pentane and (■) trichloroethylene vapor concentrations for a 97 MHz SAW device coated with a 0.70 μm-thick polyisobutylene film. A QCM coated with an identical film was used to measure the mass of absorbed vapor, from which concentration was determined.

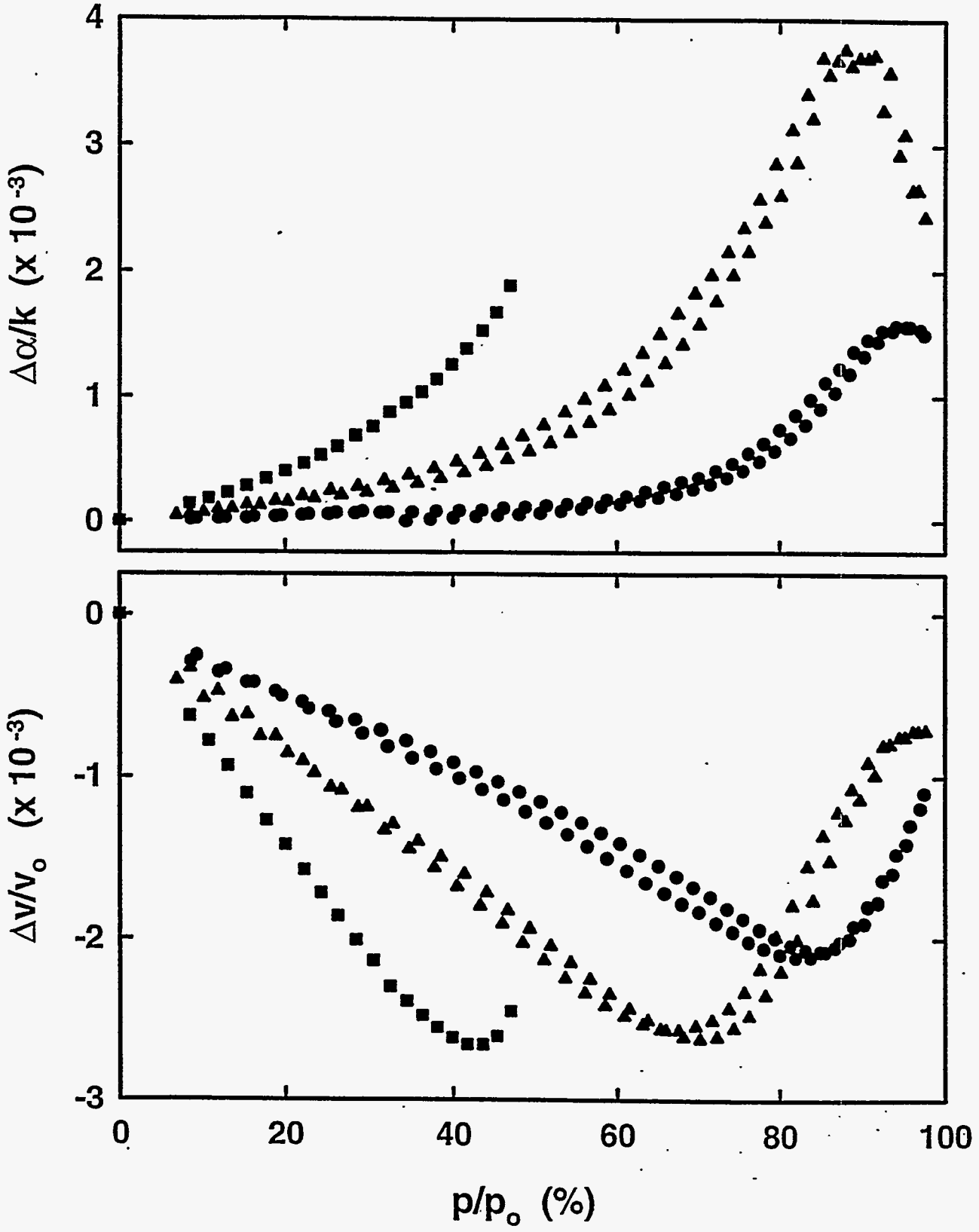

Fig. 14. Velocity and attenuation changes measured vs. relative ambient vapor pressure (p/p_o) of n-pentane with a 97 MHz SAW devices coated with polyisobutylene films of thickness: (●) 0.44, (▲) 0.73, (■) 1.18 μm.

The response is analogous to that observed as the temperature of a polymer-coated SAW device is increased. The concentration at which resonant responses arise varies inversely with the film thickness, analogous to the response vs. temperature shown in Fig. 12.

The observation of film resonances have been accentuated in this study by the unusually high vapor concentrations used in the experiments, combined with the unusually low $T_g^{(0)}$ of the polymer examined (polyisobutylene). It should be noted that for many SAW vapor sensors, film resonance effects may not be significant since (1) relatively thin films are used (<100 nm), (2) operating temperature is not as far above $T_g^{(0)}$, and (3) relatively low vapor concentrations are used (trace chemical detection).

Parametric Representation of Data

The parametric representation obtained by plotting attenuation changes vs. velocity changes facilitates comparison between data obtained in disparate experiments. Fig. 15, for example, shows parametric plots of temperature and vapor data. As the film is softened by either increasing temperature or vapor absorption, loops are formed in the parametric plots. From the calculated parametric responses of Fig. 9, in which only ϕ_3 was varied, such loops are indicative of a film resonant response occurring when ϕ_3 goes through $\pi/2$. The loops in Fig. 15 are somewhat different from those of Fig. 9, however, since increasing temperature or vapor concentration causes an increase in film lossiness (r_3) in addition to increasing ϕ_3.

The locus of points formed in the parametric plots (Fig. 15) arises from a combination of plasticizing and mass-loading responses[12]. Film softening causes an increase in ϕ_3 that generates a near-circular or spiral response. Progression around this spiral is dependent upon the free volume accumulated, either by thermal expansion or vapor absorption, in the polymer. The mass contributed by solvent absorption causes, in addition, a horizontal *translation of these points toward lower velocity*. Trichloroethylene points are translated more than pentane due to the greater density of this species. The temperature data thus represents a limiting case of vapor data in which the mass of the absorbed species is zero[12].

Multiple Film Resonances

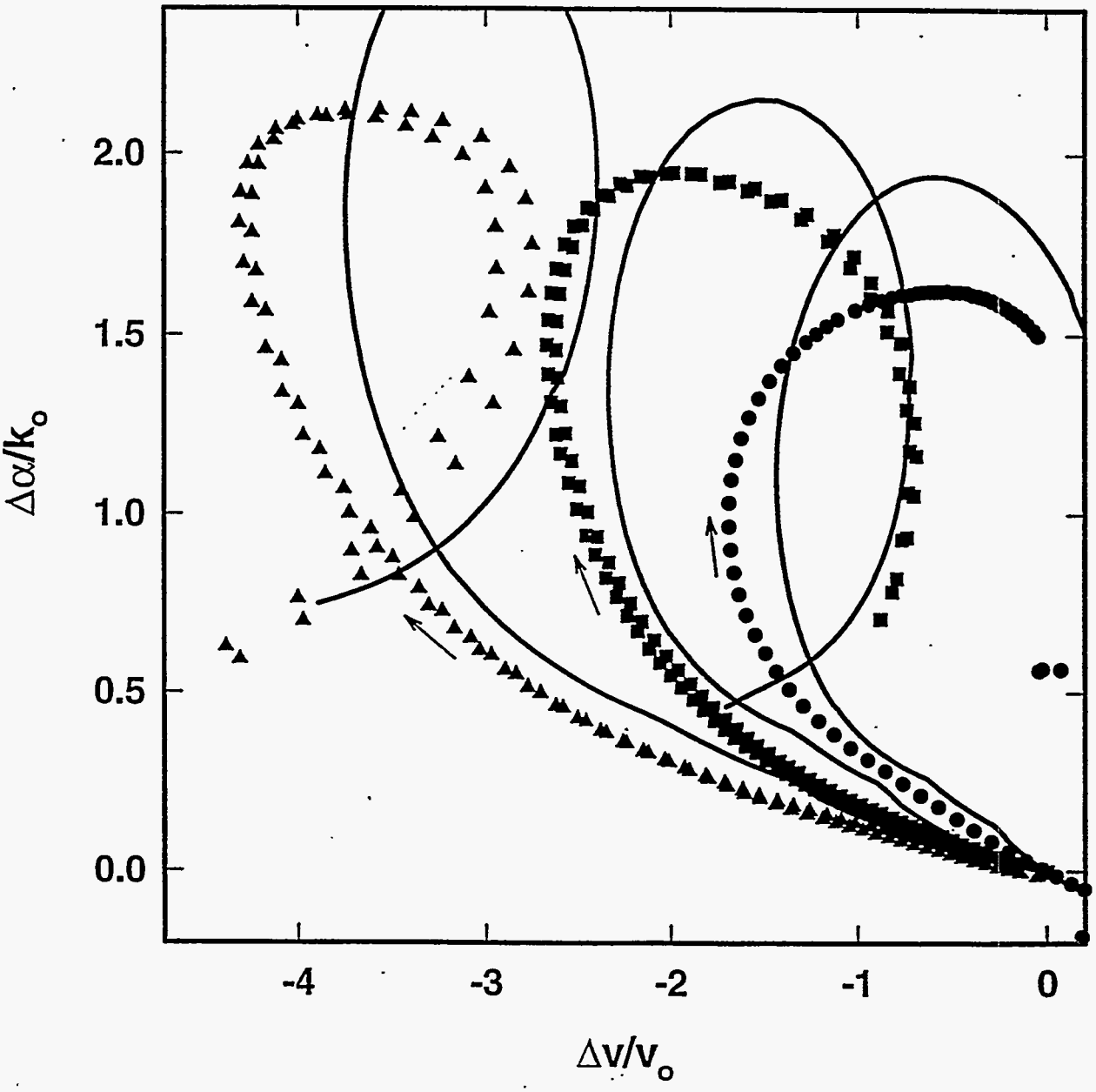

Fig. 15. Parametric plots of attenuation vs. velocity changes measured (points) and calculated (lines, Model 2) as 0.70 μm PIB films were softened by (●) increasing temperature, (■) pentane absorption, and (▲) trichloroethylene absorption. Arrows indicate increasing temperature or solvent concentration.

In our experiments with temperature cycling and vapor absorption in PIB films, only the fundamental (n=1) shear film resonance was observed. Films ranged in thickness from 0.44 to 1.43 μm; the entire resonance was not observed in the thinnest films. Ballantine[30] has reported observing fundamental film resonances at 158 MHz in PIB films only 0.0082 μm thick. For resonance to occur in films of this thickness, G' must reach values as low as 2.5×10^5 dyne/cm^2. The master curves for PIB shown in Fig. 10 indicate that this value is inaccessible at any temperature or solvent concentration. In fact, a water layer with viscosity $\eta = 1$ cP exhibits a shear modulus $G' = \omega\eta = 10^7$ dyne/cm^2 at 158 MHz. Thus, resonances should *not* occur in films this thin at 158 MHz. Ballantine also reports observing higher order film resonances (up to 9th order) in PIB. Aside from the fact that the films are much too thin for the resonance condition to be satisfied, calculations indicate that the lossiness r_3 of PIB films in the rubbery regime damps higher order film resonances too highly for them to be observed. These facts indicate that the attenuation peaks and velocity excursions reported by Ballantine are not due to film resonances.

CONCLUSIONS

Typically, polymer films on SAW devices behave as acoustically thin in the glassy regime and thick in the transition and rubbery regimes. The ratio R of in-plane to surface-normal displacement gradients, given by Eq. 4, indicates the regime of operation. In acoustically thin films, displacement is uniform across the film and varies only in the direction of propagation. In this regime, surface waves probe film viscoelastic properties mainly by imposing longitudinal strains. These cause compression and tension of the film in the direction of propagation, with corresponding expansions and contractions in film thickness. Model 1 (Eq. 5) gives the velocity and attenuation changes arising from acoustically thin viscoelastic films. (The Tiersten[14] equation (Eq. 6) is a special case of Model 1 that obtains for acoustically thin, elastic films.) When a glass transition occurs in an acoustically thin film, Model 1 indicates that an attenuation peak and velocity decrease will coincide with T_g. However, the decrease in shear modulus associated with the glass transition often causes films to behave as acoustically thick. In this regime, attenuation peaks may arise from film resonances and not just intrinsic loss peaks. This is in contrast to FPW devices on which films can behave as acoustically thin in the vicinity of T_g.

In acoustically thick films, inertially-induced lag in the film generates cross-film displacement gradients. Model 2 (Eq. 11) includes the effect of these gradients and approximates $\Delta v/v_o$ and $\Delta\alpha/k_o$ for acoustically thin or thick viscoelastic films. Table VI summarizes the extreme cases of film strain and the appropriate equations for determining $\Delta v/v_o$ and $\Delta\alpha$/k.

The emergence of film resonances complicates the extraction of T_g, which corresponds to a maximum in the intrinsic modulus G'': the temperature at which attenuation is maximum generally does *not* coincide with the intrinsic modulus maximum but depends critically on film thickness.

In the acoustically thin regime ($R \ll 1$), velocity and attenuation responses arising from vapor absorption are proportional to the species concentration in the film. These responses, previously attributed solely to mass loading, are also due in roughly equal part to polymer plasticization (softening). To obtain SAW velocity changes proportional to absorbed vapor concentration, required if the device is to respond linearly to vapor phase concentration, it is necessary that the film remain in the acoustically thin regime. The result is a tradeoff, in terms of film thickness, between sensitivity and dynamic range.

When film thickness and absorbed vapor cause R to exceed 1, the film behaves as acoustically thick. Velocity response no longer depends linearly on absorbed vapor concentration. As ϕ_3 approaches $\pi/2$, film resonance occurs and velocity increases with concentration in this regime. This makes the velocity response multi-valued: several concentrations lead to the same velocity change. By monitoring both velocity and attenuation responses, the ambiguity in concentration can be resolved.

Film resonances can be used to advantage in constructing "threshold detectors" designed for sensitivity in a specific range of vapor concentrations[30]. Film resonance effects can also be useful in providing large attenuation responses that can be used, along with the velocity response, to provide molecular discrimination and quantitation of isolated species using a single "dual output" SAW sensor[46].

A parametric plot of attenuation vs. velocity changes leads to a distinctive response when film resonance occurs: film softening causes movement around a spiral, while mass-loading translates these points toward lower velocity. The result is a characteristic loop in the $\Delta\alpha/k_o$-$\Delta v/v_o$

Table VI. Extremes of Film Strain Imposed by a SAW on a Film Overlay and the Appropriate Equations for Calculating Velocity and Attenuation Changes.

Film Condition		Principal Gradient	Appropriate Model for $\Delta v/v_o$, $\Delta\alpha/k_o$	
			Elastic	Viscoelastic
Acoustically Thin	$R \ll 1$	In-plane	Tiersten (Eq. 6) Model 1 (Eqs. 5,7) Model 2 (Eq. 11)	Model 1 (Eqs.5,7) Model 2 (Eq. 11)
Acoustically Thick	$R \geq 1$	Surface-normal	Model 2 (Eq. 11)	Model 2 (Eq. 11)

plane.

ACKNOWLEDGEMENT

The authors are grateful to B. L. Wampler of Sandia National Laboratories (SNL) for expert technical assistance and to Dr. T. Schneider and Dr. T. Tanaka of SNL and Dr. Jay Grate of Pacific Northwest Laboratories for helpful technical discussions.

CREDITS

This work was performed at SNL and supported by the U.S. Department of Energy under contract No. DE-AC04-94AL85000.

APPENDIX A: TABLE OF SYMBOLS

f_o	synchronous (center) frequency of SAW interdigital transducer
v	SAW propagation (phase) velocity
v_o	SAW propagation velocity in uncoated substrate
d	periodicity of SAW interdigital transducer
Λ	SAW wavelength (along the surface)
j	$(-1)^{1/2}$
i,j	subscripted indices with values 1,2,3, referring to x, y., and z directions, respectively
h	film thickness
h_o	film thickness at reference temperature
T_g	polymer glass transition temperature at f
$T_g^{(0)}$	polymer glass transition temperature at low frequency
α	SAW attenuation: rate of amplitude change with propagation distance
G	complex shear modulus of film ($G = G' + jG''$)
G'	shear storage modulus of film
G''	shear loss modulus of film
K	complex bulk modulus of film ($K = K' + jK''$)
K'	bulk storage modulus of film
K''	bulk loss modulus of film
$\bar{u}$	SAW displacement vector
f	excitation frequency of SAW
ω	angular excitation frequency of SAW ($2\pi f$)
t	time
γ	complex SAW propagation factor ($\gamma = \alpha + jk$)
u_i	SAW displacement in i^{th} direction
u_{io}	displacement in i^{th} direction at substrate surface
v_i	SAW particle velocity in i^{th} direction
v_{io}	particle velocity in i^{th} direction at substrate surface
ψ_i	phase of i^{th} displacement component with respect to u_z

k_o	acoustic wavenumber for SAW in uncoated substrate ($k_o = 2\pi/\Lambda = \omega/v_o$)
$\Delta\gamma/k_o$	change in complex propagation factor per wavenumber
$\Delta\alpha/k_o$	change in attenuation per wavenumber
$\Delta v/v_o$	fractional change in wave velocity
Δf	frequency change of oscillator circuit
κ	fraction of SAW wave path coated with polymer film
S_{ij}	strain tensor: $S_{ij} = 1/2(\partial u_i/\partial x_j + \partial u_j/\partial x_i)$
T_{ij}	stress tensor: force per area in the i-direction on a plane normal to the j-direction
R	ratio of strains generated by cross-film to in-plane displacement gradients
A	substrate-dependent parameter in Eq. 4 for R
ρ	film mass density
ρ_o	film mass density at reference temperature T_o
λ,μ	Lame′ constants for film
E_y, υ	Young's modulus and Poisson's ratio for film
ϕ_i	phase shift for i^{th} displacement component across film thickness
β_i	complex propagation factor for displacement u_i propagating across film
$M^{(i)}$	generalized modulus equalling G for i=1, 3 and K for i=2
$E^{(i)}$	modulus associated with film deformation generated by i^{th} displacement component
r_i	film loss parameter associated with displacement component u_i
$\hat{x}_i$	unit displacement vector in i-direction
$\Delta\rho$	change in film mass density
$\Delta G'$	change in shear storage modulus of film
$\Delta G''$	change in shear loss modulus of film
c_i	ratio of particle velocity (squared) at substrate surface to acoustic power flow: $c_i = v_{io}^2/(4k_o P)$
P	SAW acoustic power density (power per beamwidth)
a,b	film-dependent parameters in ϕ_3 and r_3 expressions (eqs. 9 and 10)
n	film resonance harmonic number
Z_i	surface mechanical impedance in ith direction at substrate/film interface
Re	denotes the real part of a complex expression

Im	denotes the imaginary part of a complex expression
ω'	apparent probe frequency of SAW
a_T	shift factor for polymer relaxation or ω' due to temperature change or vapor absorption
F	free volume of polymer at any temperature or vapor concentration
F_o	free volume of pure polymer (C = 0) at reference temperature
B	constant in generalized Doolittle equation, taken as unity
ξ	parameter describing extent to which free volume addition swells film
α_f	polymer thermal expansion coefficient
Δh	change in film thickness due to temperature change or vapor absorption
F_g	free volume of polymer at $T_g^{(0)}$
χ	plasticizing parameter for polymer
V_1	volume fraction of absorbed vapor in polymer
C	concentration of absorbed vapor relative to pure polymer
m	specific mass of absorbed vapor
V	specific volume of absorbed vapor
δ	liquid density of vapor
ΔL	change in insertion loss (in decibels)
N_A	no. of SAW wavelengths separating interdigital transducers (center-to-center)
T	temperature
T_o	reference temperature (film formation temperature)
$\mathfrak{u}(y)$	cross-film displacement vector
$S^{(IP)}$	total strain induced by in-plane (IP) gradients
$S^{(CF)}$	total strain induced by cross-film (CF) gradients
δ_{ij}	Kronecker delta function: equal to 1 when $i = j$ and 0 otherwise

Appendix B: Ratio of Film Strains Generated by SAW-Induced Cross-Film Gradients to In-Plane Gradients

SAW propagation in the z-direction of a film-coated substrate causes film displacements given by:

$$\vec{u} = \hat{u}(y)\, e^{j(\omega t - kz)} \tag{B1}$$

where y is distance across the film, $\hat{u}(y)$ is the cross-film displacement, ω is the angular frequency ($\omega = 2\pi f$), and k is the SAW wavenumber ($k = 2\pi/\Lambda = \omega/v_o$). In-plane gradients arise from harmonic variation in the z-direction, described by the exponential term in Eq. B1. Cross-film gradients arise from variations in $\hat{u}(y)$ arising from inertial lag of the upper film portions with respect to the driven lower film surface.

Strains due to in-plane gradients If we assume that $\hat{u}(y)$ is constant across the film thickness, film strains, $S_{ij} = 1/2(\partial u_i/\partial x_j + \partial u_j/\partial x_i)$, are then generated only by the harmonic variation of $\vec{u}$ in the z-direction:

$$S_{i3} = \frac{1}{2}\frac{\partial u_i}{\partial z} = -\frac{jku_i}{2} \tag{B2}$$

for $i = 1, 2, 3$. S_{13} and S_{23} are shear strains and S_{33} is a tensile strain. The magnitude of the total strain induced by in-plane (IP) gradients is

$$S^{(IP)} = \frac{k}{2}\left(u_{xo}^2 + u_{yo}^2\right)^{1/2} + ku_{zo} \tag{B3}$$

where the uniform film displacements u_i have been replaced by the displacements at the substrate/film interface, u_{io}.

B. Strains due to cross-film gradients When the lower film surface undergoes SAW-induced displacement, the inertial lag of the upper film portions causes $\hat{u}(y)$ in Eq. B1 to vary across the film. However, shear wave velocity is low enough that gradients of u_x and u_z arise, leading to shear strains in the film. The continuity equation gives:

$$\sum_{j=1}^{3} \frac{\partial T_{ij}}{\partial x_j} = \rho \dot{v}_i = -\rho \omega^2 u_i \qquad \text{(B4)}$$

where particle velocity $v_i = \dot{u}_i = j\omega u_i$, T_{ij} is the stress (force per area in the i-direction on a plane normal to the j-direction), and ρ is film density. Since the upper film surface is stress-free, i.e., $T_{i2}(h) = 0$, we can approximate the derivative in Eq. B4 as $\partial T_{i2}/\partial x_2 \cong -T_{i2}(0)/h$; h is film thickness. Then the stresses required at the substrate/film interface to drive the film can be found from Eq. B4:

$$T_{i2}(0) = \rho \omega^2 h u_{io} \qquad \text{(B5)}$$

for $i = 1$ and 3. The shear strains S_{ij} in the film are related to shear stresses by $T_{ij} = 2GS_{ij}$ (for $i \neq j$), where G is the film's shear modulus. From Eq. B5, the film shear strains (at the lower film surface) are

$$S_{i2}(0) = \frac{T_{i2}(0)}{2G} = \frac{\rho \omega^2 h u_{io}}{2G} \qquad \text{(B6)}$$

for $i = 1, 3$. The magnitude of the total strain induced by inertially generated cross-film (CF) gradients is then

$$S^{(CF)} = \frac{\rho \omega^2 h}{2|G|} \left(u_{xo}^2 + u_{zo}^2 \right)^{1/2} . \qquad \text{(B7)}$$

The ratio of strain magnitudes induced by cross-film to in-plane gradients is found by combining Eqs. B3 and B7:

$$R = \frac{S^{(CF)}}{S^{(IP)}} = \left(\frac{(c_1 + c_3)^{1/2}}{(c_1 + c_2)^{1/2} + 2c_3^{1/2}} \right) \frac{\omega v_o \rho h}{|G|} = \frac{A f v_o \rho h}{|G|} \qquad \text{(B8)}$$

where we have defined $A \equiv 2\pi(c_1 + c_3)^{1/2}/[(c_1 + c_2)^{1/2} + 2c_3^{1/2}]$ and used the definition $c_i = v_{io}^2/(4k_o^2 P) = (\omega u_{io})^2/(4k_o^2 P)$, where v_{io} is the surface particle velocity and P is the SAW acoustic power density (R is independent of P). Taking c_i values from Table II, $A \cong 1.9$ for propagation in the X-direction of ST-cut quartz.

Appendix C: SAW Loading by an Acoustically Thin Viscoelastic Layer

A perturbational method can be applied to approximate the changes in SAW propagation velocity and attenuation contributed by an acoustically thin viscoelastic surface film: changes in the complex propagation factor γ are related to the surface mechanical impedances Z_i experienced by the surface displacement components u_{io} in translating and deforming the film overlay[23]:

$$\frac{\Delta\gamma}{k_o} = \frac{\Delta\alpha}{k_o} - j\frac{\Delta v}{v_o} = \sum_{i=1}^{3} c_i Z_i \qquad \text{(C1)}$$

where c_i are the normalized surface particle velocities (defined in Appendix B) and the surface mechanical impedances are[23]

$$Z_i = -\frac{T_{i2}}{v_i}\bigg|_{y=0} \qquad \text{(C2)}$$

where T_{i2} and v_i, evaluated at $y = 0$, denote interfacial stress (defined in Appendix B) and particle velocity in the i-direction, respectively. For an isotropic film, the displacement components can be considered independently in calculating Z_i.

For an acoustically thin ($R \ll 1$) film, displacements can be assumed uniform across the film thickness: $u_i = u_{io}$. Applying the continuity equation (Eq. B4), and assuming uniform wave displacement in the x-direction ($\partial T_{i1}/\partial x_1 = 0$), yields

$$\frac{\partial T_{i2}}{\partial y} + \frac{\partial T_{i3}}{\partial z} = \rho\dot{v}_i \qquad \text{(C3)}$$

for $i = 1, 2, 3$; ρ is film density. Since wave variations in the x direction are zero, The upper film surface is stress-free so that $T_{i2}(h) = 0$, allowing an approximation for the first term of Eq. C3:

$$\frac{\partial T_{i2}}{\partial y} \cong -\frac{T_{i2}(0)}{h} \qquad \text{(C4)}$$

We define a deformation modulus relating stress (generated by displacement component x_i) to strain:

$$E_i = \left(\frac{1 + \delta_{i3}}{2} \right) \frac{T_{i3}}{S_{i3}} \tag{C5}$$

where $\delta_{i3} = 1$ if $i = 3$ and zero otherwise. Then we can write the second term of Eq. C3 as:

$$\frac{\partial T_{i3}}{\partial z} = E^{(i)} \frac{\partial^2 u_i}{\partial z^2} \quad . \tag{C6}$$

Using Eqs. C4 and C6 in Eq. C3 yields:

$$\frac{T_{i2}(0)}{h} = E^{(i)} \frac{\partial^2 u_i}{\partial z^2} - \rho \ddot{u}_i \tag{C7}$$

giving a one-dimensional wave equation in the film overlay. The SAW-supplied stress $T_{i2}(0)$, applied at the lower film surface, acts as a *source* for this wave. Noting from Eq. B1 that $\ddot{u}_i = (j\omega)^2 u_i$ and $\partial^2 u_i/\partial z^2 = (-jk)^2 u_i = -k^2 u_i$, Eq. C7 becomes

$$T_{i2}(0) = h\left(\rho\omega^2 - k^2 E^{(i)}\right) u_{io} \quad . \tag{C8}$$

Using Eq. C8 in Eq. C2, and noting that $v_i = j\omega u_i$ and $\gamma = \omega/k$, yields the surface mechanical impedance components:

$$Z_i = j\omega h \left(\rho - \frac{E^{(i)}}{v_o^2} \right) \tag{C9}$$

where v_o is the unperturbed SAW propagation velocity. The first term of Eq. C9 is a kinetic contribution, while the second term arises from straining the film overlay.

Substituting Eq. C9 into Eq. C1 yields the perturbation in SAW propagation characteristics arising from an acoustically thin ($R \ll 1$) viscoelastic film overlay:

$$\frac{\Delta\gamma}{k_o} = \frac{\Delta\alpha}{k_o} - j\frac{\Delta v}{v_o} = j\omega h \sum_{i=1}^{3} c_i \left(\rho - \frac{E^{(i)}}{v_o^2} \right) \tag{C10}$$

with c_i as given in Appendix B or Table II.

We examine a single deformation mode to illustrate the calculation of the deformation moduli $E^{(i)}$ involved in Eq. C10. Deformation is assumed to be uniform across the film, as shown in Fig. 4, consistent with the assumption of acoustic thinness. The compressional modulus $E^{(3)}$, for example, can be related to intrinsic elastic film properties by simultaneously solving the plane-strain relations[47]:

$$T_{33} = \left(K - \frac{2}{3} G \right) \left(S_{22} + S_{33} \right) + 2GS_{33} \tag{C11a}$$

$$T_{22} = \left(K - \frac{2}{3}G\right)\left(S_{22} + S_{33}\right) + 2GS_{22} \tag{C11b}$$

where K and G are the bulk and shear moduli, respectively, of the film overlay. Since the upper film surface is stress-free, $T_{22} = 0$, allowing Eq. C11b to be solved for S_{22}:

$$S_{22} = -\left(\frac{K - \frac{2}{3}G}{K + \frac{4}{3}G}\right)S_{33} \tag{C12}$$

Substituting Eq. C12 into Eq. C11a yields the compressional modulus defined by Eq. C5:

$$E^{(3)} = \frac{T_{33}}{S_{33}} = \frac{4G(3K + G)}{3K + 4G} \tag{C13}$$

The moduli $E^{(1)}$ and $E^{(2)}$ can be derived in a similar manner to produce:

$$E^{(1)} = \frac{T_{13}}{2S_{13}} = G \tag{C14a}$$

$$E^{(2)} = \frac{T_{23}}{2S_{23}} = \frac{2\pi G(G + 3K)}{3(4G + K)}\left(\frac{h}{\Lambda}\right)^2 \tag{C14b}$$

where Λ is the SAW wavelength. Typically the modulus $E^{(2)}$ is negligible, due to the $(h/\Lambda)^2$ term, and is taken as zero.

Appendix D: SAW Loading by an Acoustically Thick Viscoelastic Layer

A perturbational method is applied to approximate the changes in SAW propagation velocity and attenuation contributed by an acoustically thick ($R \geq 1$) viscoelastic film. By considering both in-plane and cross-film displacement gradients, the final result applies to both acoustically thin and thick films. Changes in the complex propagation factor γ are related to the surface mechanical impedances Z_i by Eq. C1. In calculating the surface mechanical impedances, the SAW surface

displacement is resolved into surface-normal and in-plane components; these act as *sources* for radiating waves into the contacting film. A distributed model is used for the film, in which the impedance at the lower film surface depends upon the nature of the interference between the incident waves and those reflected from the upper (film/air) surface.

As in the acoustically thin case (Appendix C), the displacement components are considered independently in calculating surface mechanical impedances. Assuming no wave variation in the x-direction, the continuity equation (Eq. B4) gives:

$$\frac{\partial T_{i2}}{\partial y} + \frac{\partial T_{i3}}{\partial z} = \rho \dot{v}_i \tag{D1}$$

for $i = 1, 2, 3$. From Eq. C5, in-plane displacement gradients in the film gives rise to

$$T_{i3} = E^{(i)} \frac{\partial u_i}{\partial z} \tag{D2}$$

with $E^{(i)}$ given by Eqs. C13, C14. Cross-film gradients give rise to

$$T_{i2} = M^{(i)} \frac{\partial u_i}{\partial y} \tag{D3}$$

where $M^{(1)} = M^{(2)} = G$, while $M^{(3)} = K$. Substituting Eqs. D2 and D3 into D1 yields a two-dimensional wave equation for the displacement u_i in the film:

$$M^{(i)} \frac{\partial^2 u_i}{\partial y^2} + E^{(i)} \frac{\partial^2 u_i}{\partial z^2} = \rho \dot{v}_i \quad . \tag{D4}$$

Substituting the harmonic solution for the z-propagating wave (Eq. B1) into Eq. D4 yields a homogeneous ordinary differential equation for the displacement profile $u_i(y)$ in the film:

$$\frac{d^2 u_i}{dy^2} + \beta_i^2 u_i = 0 \tag{D5a}$$

with

$$\beta_i = \omega \left(\frac{\rho - E^{(i)}/v_o^2}{M^{(i)}} \right)^{\frac{1}{2}} \tag{D5b}$$

where $v_o = \omega/k$ is the unperturbed SAW phase velocity. The solution to Eq. D5a for $0 \le y \le h$ is

$$u_i(y) = A e^{j\beta_i y} + B e^{-j\beta_i y} \tag{D6}$$

where h is film thickness and A and B are constants. The factors β_i are propagation constants describing wave propagation across the film. For a viscoelastic material, characterized by complex bulk and shear moduli (K and G), β_i are complex.

The constants A and B in Eq. D6 are determined from the boundary conditions that apply at the upper and lower film surfaces. The first boundary condition stipulates that the displacement at the film/substrate interface be continuous, i.e., $u_i(0^+) = u_{io}$, where $u_i(0^+)$ is the displacement at the lower film surface. Eq. D6 gives

$$A + B = u_{io} \quad . \tag{D7}$$

The second boundary condition stipulates that the upper film surface (film/air interface) be stress-free: $T_{i2}(h) = 0$. Evaluating Eq. D3 at $y = h$, with u_z given by Eq. D6, gives:

$$A e^{j\beta_i h} - B e^{-j\beta_i h} = 0 \quad . \tag{D8}$$

Solving Eqs. D7 and D8 simultaneously determines A and B:

$$A = \frac{u_{io} e^{-j\beta_i h}}{e^{j\beta_i h} + e^{-j\beta_i h}} \tag{D9a}$$

Substituting Eqs. D9 into D6 determines the displacement profiles $u_i(y)$ across the film: for $0 \le y \le h$.

$$B = \frac{u_{io}\, e^{j\beta_i h}}{e^{j\beta_i h} + e^{-j\beta_i h}} \tag{D9b}$$

$$u_i(y) = u_{io} \frac{\cosh\left[j\beta_i(y-h)\right]}{\cosh(j\beta_i h)} \tag{D10}$$

The surface mechanical impedance associated with each displacement u_i is given by Eq. C2. In evaluating this impedance, the interfacial shear stress is found from Eq. D3, using Eq. D6 for u_i:

$$T_{i2}(0) = M^{(i)} \frac{\partial u_i}{\partial y}\Big|_{y=0} = j\beta_i M^{(i)}(A - B) \tag{D11}$$

and the interfacial particle velocity is found from Eq. D6:

$$v_i(0) = \dot{u}_i(0) = j\omega u_i(0) = j\omega(A + B) \quad . \tag{D12}$$

Substituting Eqs. D11 and D12 into Eq. C2, and using Eq. D9 for A and B, gives the surface mechanical impedance associated with each displacement u_i:

$$Z_i = -\frac{\beta_i M^{(i)}}{\omega}\left(\frac{A - B}{A + B}\right) = \frac{\beta_i M^{(i)}}{\omega} \tanh(j\beta_i h) \quad . \tag{D13}$$

From Eq. C1, the perturbation in SAW propagation arising from a viscoelastic film is determined from the surface mechanical impedances (Eq. D13):

$$\frac{\Delta\gamma}{k_o} = \frac{\Delta\alpha}{k_o} - j\frac{\Delta v}{v_o} = \sum_{i=1}^{3} \frac{c_i \beta_i M^{(i)}}{\omega} \tanh(j\beta_i h) \tag{D14}$$

with β_i as given in Eq. D5b and c_i and $E^{(i)}$ values as given in Appendix C and Tables I and II. Eq. D14 applies for acoustically thin or thick films (all R-values).

LITERATURE CITED

(1) White, R. M.; Volltmer, F. W. *Appl. Phys. Lett.* **1965**, *7*, 314.

(2) The Euler angles for ST-cut quartz are 0°, 132.75°, 0°. SAW velocity in the X-propagation direction is 3.158×10^5 cm/s.

(3) Datta, S. *Surface Acoustic Wave Devices*, Prentice-Hall: Englewood Cliffs, NJ, 1986.

(4) (a) Hickernell, F. S.; Wagers, R. S. *IEEE 1984 Ultrasonics Symposium Proceedings* (IEEE, New York, 1984) 253-257. (b) Wagers, R. S. *IEEE 1980 Ultrasonics Symposium Proceedings* (IEEE, New York, 1980) 464-469. (c) Ricco, A. J.; Martin, S. J. *Sensors and Actuators* B (Chemical) **1993**, *B10* (2), 123-31.

(5) (a) Wohltjen, H.; Dessey, R. *Anal. Chem.*, **1979**, *51*, 1458-1464. (b) Wohltjen, H.; Dessey, R. *Anal. Chem.*, **1979**, *51*, 1465-1470. (c) Frye, G. C.; Martin, S. J.; Cernosek, R. W.; Pfeifer, K. B.; Anderson, J. S. *IEEE 1991 Ultrasonics Symposium Proceedings* (IEEE, New York, 1991) 311-16. (d) Watson, G.; Horton, W.; Staples, E. *IEEE 1992 Ultrasonics Symposium Proceedings*, IEEE Cat. no. 92CH3118-7 (IEEE, New York, 1992) 269-273. (e) Bowers, W. D.; Chuan, R. L., Duong, T. M. *Rev. Sci. Instrum.* **1991**, *62*(6), 1624-1629. (f) Arn, D.; Amati, D.; Blom, N.; Ehrat, M.; Widmer, H. M. *Sensors and Actuators B*, **1992**, *8*, 27-31.

(6) Wohltjen, H.; U. S. Patent 4,312,228 (Jan. 26, 1982).

(7) (a) Ballantine, D. S.; Wohltjen, H. *Anal. Chem.* **1989**, *61*(11), 704A-715A. (b) Nieuwenhuizen, M. S.; Barendsz, A. W. *Sensors and Actuators* **1987**, *11*, 45-62. (c) White, R. M.; Wicher, P. J.; Wenzel, S. W.; Zellers, E. T. *IEEE Trans. on UFFC* **1987**, *UFFC-34*, 162-171. (d) Brace, J. G.; Sanfelippo, T. S.; *Sensors and Actuators* **1988**, *14*, 47-68. (e) Galipeau, D. W., Feger, C.; Vetelino, J. F.; Lec, R. IEEE 1990 Ultrasonics

Symposium Proceedings (IEEE, New York, 1990) 1087-90. (f) Gizeli, E.; Goddard, N. J.; Lowe, C. R.; Stevenson, A. C. *Sensors and Actuators* B (Chemical) **1992**, *B6* (1-3), 131-137. (g) Mizutani, F.; Yoshino, I.; Tamura, M; Yoshida, T. *Koatsu Gasu* **1990**, *27* (5), 339-43. (h) Wenzel, S. W.; White, R. M. *Sensors and Actuators* **1990**, *A21-A23*, 700-703. (i) Katritzky, A. R.; Savage, G. P.; Pilarska, M. *Talanta*, **1991**, *38*, 201-204. (j) Chang, S.; Tamiya, E.; Karube, I. *Biosensors and Bioelectronics*, **1991**, *6*, 9-14. (k) Grate, J. W.; McGill, R. A.; Abraham, M. H. *IEEE 1992 Ultrasonics Symposium Proceedings*, IEEE Cat. no. 92CH3118-7 (IEEE, New York, 1992) 275-279. (l) Goydan, R.; Reid, R. C.; Tseng, H. S. *Ind. Eng. Chem. Res.* **1989**, *28*, 445-454. (m) Grate, J. W.; Abraham, M. H. *Sensors and Actuators* B Chemical **1991**, *3*, 85-111. (n) Ballantine, D.S.; Rose, S.L.; Grate, J. W.; Wohltjen, H. *Anal. Chem.* **1986**, *58*, 3058-3066. (o) Carey, W. P.; Kowalski, B. R. *Anal. Chem.* **1986**, *58*, 3077-3084. (p) Rose-Pehrsson, S. L.; Grate, J. W.; Ballantine, D. S.; Jurs, P. C. *Anal. Chem.* **1988**, *60*, 2801-2811. (q) Schmautz, A. *Sensors and Actuators B*, **1992**, *6*, 38-44.

(8) Sugimoto, I.; Nakamura, M.; Kuwano, H. *Proc. Transducers '91*, IEEE: New York, 1991, 994-997.

(9) Ferry, J. D. *Viscoelastic Properties of Polymers*, 3rd ed, Wiley: New York, 1980, Ch. 1.

(10) Lewis, A. F. *Polymer Letters* **1963**, *1*, 649-654.

(11) (a) Ballantine, D. S.; Wohltjen, H. *Chemical Sensors and Microinstrumentation, ACS Symposium Series 403*, American Chemical Society: Washington, DC, 1989, 222-236. (b) Wohltjen, H.; Dessey, R. *Anal. Chem.*, **1979**, *51*, 1470-1475. (c) Wohltjen, H.; Dessy, R.; *Anal. Chem.* **1979**, *51* 1470-1475. (d) Groetsch, J. A.; Dessy, R. E. *J. Appl. Polymer Sci.*

1983, *28*, 161-178. (e) Caliendo, C.; Fioretto, C.; Socino, G.; Verona, E. *IEEE 1991 Ultrasonics Symposium Proceedings* (IEEE, New York, 1991), 387-391.

(12) Martin, S. J.; Frye, G. C. *Appl. Phys. Lett.* **1990**, *57*, 1867-1869.

(13) Grate, J. W.; Wenzel, S. W.; White, R. M. *Anal. Chem.* **1992**, *64*, 413-423.

(14) Tiersten, H. F.; Sinha, B. K. *J. Appl. Phys.* **1978**, *49*(1), 87-95.

(15) Skeie, H.; *J. Acous. Soc. Am.* **1970**, *48*, 1098-1109.

(16) Wolkerstorfer, D. C. "Methods for Measuring the Acoustic and Optical Properties of Organic Crystals," PhD Thesis, Stanford Univ., Aug. 1971.

(17) (a) Wohltjen, H.; Snow, A. W.; Barger, W. R.; Ballantine, D. S. *IEEE Trans. on UFFC* **1987**, *UFFC-34*, 172-178. (b) Grate, J. W.; Klusty, M. *Anal. Chem.* **1991**, *63*, 1719-1727.

(18) Wohltjen, H. *Sensors and Actuators* **1984**, *5*, 307.

(19) Frye, G. C.; Martin, S. J. *Sensors and Materials* **1991**, *2*, 187-195.

(20) Ferry, J. D. *Viscoelastic Properties of Polymers*, 3rd ed, Wiley: New York, 1980, Ch. 17.

(21) Grate, J. W.; Snow, A.; Ballantine, D. S.; Wohltjen, H.; Abraham, M. H.; McGill, R. A.; Sasson, P. *Anal. Chem.*, **1988**, *60*, 869-875.

(22) Grate, J. W.; Klusty, M.; McGill, R. A.; Abraham, M. H.; Whiting, G.; Andonian-Haftvan, J. *Anal. Chem.* **1992**, *64*, 610-625.

(23) Auld, B. A. *Acoustic Fields and Waves in Solids*, vol. II, Wiley: New York, 1973, Ch. 12.

(24) Auld, B. A. *Acoustic Fields and Waves in Solids*, vol. II, Wiley: New York, 1973, Ch. 1.

(25) Martin, S. J.; Ricco, A. J. *Proceedings of the IEEE Ultrasonics Symposium*, 1989, 621-625.

(26) Landau, L. D.; Lifshitz, E. M. *Theory of Elasticity*, 3rd Ed., Pergamon: New York, 1986, Ch. 1.

(27) Brekhovskikh, L.; Goncharov, V. *Mechanics of Continua and Wave Dynamics*, Sprinter-Verlag: New York, 1982, sec. 3.4.

(28) Slobodnik, A. J.; Conway, E. D.; Delmonico, R. T. *Microwave Acoustics Handbook, Vol 1A, Surface Wave Velocities*, National Technical Information Service, Washington, DC, 1973.

(29) Martin, S. J.; Frye, G. C. *1991 Ultrasonics Symposium Proceedings* (IEEE, New York, 1991) 393-398.

(30) Ballantine, D. S. *Anal. Chem.* **1992**, *64*, 3069-3076.

(31) Frederick, D. K.; Carlson, A. B. *Linear Systems in Communication and Control*, Wiley: New York, 1971, Ch. 11.

(32) Cole, R. H.; Cole, K. S. *J. Chem. Phys.* **1941**, *9*, 341.

(33) Marvin, R. S.; Aldrich, R.; Sack, H. S.; *J. Appl. Phys.* **1954**, *25* (10), 1213-1218.

(34) Ferry, J. D. *Viscoelastic Properties of Polymers*, 3rd ed; Wiley: New York, 1980, Appendix D.

(35) Aklonis, J. J.; MacKnight, W. J. *Introduction to Polymer Viscoelasticity*, Wiley: New York, 1983, Ch. 3.

(36) Williams, M. L.; Landel, R. F.; Ferry, J. D. *J. Amer. Chem. Soc.* **1955**, *77*, 3701.

(37) Doolittle, A. K.; Doolittle, D. B. *J. Appl. Phys.* **1959**, *31*, 1164.

(38) Bartley, D. L.; Dominguez, D. D. *Anal. Chem.* **1990**, *62*, 1649-1656.

(39) $F_o = F_g + \alpha_f(T_o - T_g^{(0)})$, where F_g is the free volume at the glass transition temperature $T_g^{(0)}$ with no in-plane stresses.

(40) Grate, J. W. "Sensing Glass Transitions in Thin Polymer Films on Acoustic Wave Microsensors, " ASTM Special Technical Publication on Assignment of the Glass

Transition, in Press.

(41) Frye, G. C.; Martin, S. J. *Applied Spectroscopy Reviews* **1991**, *26*(1&2), 73-149.

(42) Only selected data points are shown; data is available from the authors on request.

(43) Morgan, D. P. *Surface-Wave Devices for Signal Processing* Elsevier: New York, 1985, Sec. 6.4.

(44) (a) Wenzel, S. W.; White, R. M. *IEEE Trans. Electron Devices* **1988**, *ED-35*, 735-743. (b) Wenzel, S. W.; White, R. M. *Sensors and Actuators* **1990**, *A21-A23*, 700-703.

(45) Weast, R. C.; Astle, M. J.; Beyer, W. H. *CRC Handbook of Chemistry and Physics*; CRC Press: Boca Raton, FL, 1983.

(46) Frye, G. C.; Martin, S. J.; Cernosek, R. W.; Pfeifer, K. B.; Anderson, J. S. *1991 Ultrasonics Symposium Proc.*, IEEE: New York, 1991, 311-316.

(47) Lai, W. M.; Krempl, E. *Introduction to Continuum Mechanics*, Pergamon: New York, 1974.

(48) Ferry, J. D. *Viscoelastic Properties of Polymers*, 3rd ed; Wiley: New York, 1980, Appendix D.

DISTRIBUTION:

2	MS1425	G. C. Frye, 1315
1	MS1425	S. J. Martin, 1315
1	MS1425	R. Kottenstette, 1315
1	MS0188	LDRD Office, 4523
1	MS9018	Central Technical Files, 8940-2
5	MS0899	Technical Library, 4414
2	MS0619	Review & Approval Desk, 12690